

Library copy
RD 1546

~~CONFIDENTIAL~~

Copy 44
RM SL51E22

N-5026

C. 2

NACA

RESEARCH MEMORANDUM

for the

Bureau of Aeronautics, Department of the Navy

TRANSONIC STABILITY AND CONTROL INVESTIGATION

OF A $\frac{1}{80}$ -SCALE MODEL OF THE CONSOLIDATED

VULTEE SKATE 9 SEAPLANE

TED NO. NACA DE 345

TRANSONIC-BUMP METHOD

By John M. Riebe and Richard G. MacLeod

Langley Aeronautical Laboratory
Langley Field, Va.

Restriction/Classification Cancelled

This document contains information of the Espionage
manner to an unauthorized person.

United States within the
of its contents in any

Information so classified may be imparted only to persons in the military and naval services of the United States, appropriate civilian officers and employees of the Federal Government who have a legitimate interest therein, and to United States citizens of known loyalty and discretion who of necessity must be informed thereof.

NATIONAL ADVISORY COMMITTEE FOR AERONAUTICS

WASHINGTON

~~CONFIDENTIAL~~



NATIONAL ADVISORY COMMITTEE FOR AERONAUTICS

RESEARCH MEMORANDUM

for the

Bureau of Aeronautics, Department of the Navy

TRANSONIC STABILITY AND CONTROL INVESTIGATION

OF A $\frac{1}{80}$ -SCALE MODEL OF THE CONSOLIDATED

VULTEE SKATE 9 SEAPLANE

TED NO. NACA DE 345

TRANSONIC-BUMP METHOD

By John M. Riebe and Richard G. MacLeod

SUMMARY

An investigation of the longitudinal stability and of the all-movable horizontal tail and aileron control of a $\frac{1}{80}$ -scale reflection-plane model of the Consolidated Vultee Skate 9 seaplane has been made through a Mach number range of 0.6 to 1.16 on the transonic bump of the Langley high-speed 7- by 10-foot tunnel.

At moderate lift coefficients (0.4 to 0.8) and below a Mach number of 1.0 the model was statically unstable longitudinally. The static longitudinal stability of the model at low lift coefficients increased with Mach number corresponding to a shift in aerodynamic center from 37 percent mean aerodynamic chord at a Mach number of 0.60 to 64 percent at a Mach number of 1.10. Estimates indicate that the tail deflection angle required for steady flight and for accelerated maneuvers of the Skate 9 airplane would probably not vary greatly with Mach number at sea level, but for accelerated maneuvers at altitude the tail deflection angle would probably vary erratically with Mach number.

The variation of rolling-moment coefficient with aileron deflection angle was approximately linear, agreed well with theory, and held for the range of aileron deflections tested (-17.1° to 16.6°).

~~CONFIDENTIAL~~

At low lift coefficients the drag rise occurred at Mach numbers of 0.95 and 0.90 for the wing alone and the complete model, respectively.

The effects of the canopy on the model were small. For the ranges investigated, angle-of-attack and Mach number changes caused no large pressure drops in the jet-engine duct.

INTRODUCTION

An investigation of the longitudinal stability and control and of the aileron control characteristics of a $\frac{1}{80}$ -scale reflection-plane model of the Consolidated Vultee Skate 9 high-speed seaplane has been made on the transonic bump of the Langley high-speed 7- by 10-foot tunnel. The investigation was requested by the Bureau of Aeronautics, Department of the Navy.

The Skate seaplane incorporated a hull which was blended into the wing. Results of a reflection-plane-model investigation, up to a Mach number of 0.98, of a blended hull which was somewhat similar to the Skate model are presented in reference 1.

The present paper contains the aerodynamic characteristics of the Skate model and its component parts through a -21° to 26° angle-of-attack range and in a 0.6 to 1.16 Mach number range. A limited investigation was also made of the air flow in the jet-engine duct through the same range of angle of attack and Mach number.

COEFFICIENTS AND SYMBOLS

C_L	lift coefficient $\left(\frac{\text{Twice lift of semispan model}}{qS} \right)$
C_D	drag coefficient $\left(\frac{\text{Twice drag of semispan model}}{qS} \right)$
C_l	rolling-moment coefficient at plane of symmetry $\left(\frac{\text{Rolling moment of semispan model}}{qSb} \right)$
C_{l_a}	rolling-moment coefficient produced by one aileron (rolling-moment coefficient of entire wing with one aileron deflected minus rolling-moment coefficient of entire wing with undeflected aileron)

- C_n yawing-moment coefficient $\left(\frac{\text{Yawing moment of semispan model}}{qSb} \right)$
- C_{na} yawing-moment coefficient produced by one aileron (yawing-moment coefficient of entire wing with one aileron deflected minus yawing-moment coefficient of entire wing with undeflected aileron)
- C_m pitching-moment coefficient about center-of-gravity location (0.25 \bar{c}) shown in figure 1
 $\left(\frac{\text{Twice pitching moment of semispan model}}{qS\bar{c}} \right)$
- q effective dynamic pressure over span of model, pounds per square foot $\left(\frac{1}{2} \rho V^2 \right)$
- S twice wing area of semispan model, 0.158 square foot
- b twice span of semispan model, 0.797 foot
- \bar{c} mean aerodynamic chord of wing, 0.211 foot based on relationship $\left(\frac{2}{S} \int_0^{b/2} c^2 dy \right)$
- c local wing chord, feet
- y lateral distance from plane of symmetry
- ρ mass density of air, slugs per cubic foot
- V free-stream air velocity corresponding to effective Mach number, feet per second
- M effective Mach number over span of model
- M_a average chordwise local Mach number
- M_l local Mach number
- R Reynolds number of wing based on \bar{c}
- α angle of attack, referred to wing-chord line, degrees
- δ aileron deflection relative to wing-chord plane measured perpendicular to control hinge axis, positive trailing edge down, degrees

δ_t tail deflection angle with respect to wing chord line,
positive trailing edge down, degrees

$$C_{L_\alpha} = \left(\frac{\partial C_L}{\partial \alpha} \right)_\delta$$

$$C_{l_\delta} = \left(\frac{\partial C_l}{\partial \delta} \right)_\alpha$$

$$C_{n_\delta} = \left(\frac{\partial C_n}{\partial \delta} \right)_\alpha$$

MODEL AND APPARATUS

The $\frac{1}{80}$ -scale semispan model of the Consolidated Vultee Skate 9 seaplane used in the investigation (figs. 1 and 2 and table I) had a 40° sweptback wing with a dihedral angle of $2^\circ 33'$, a taper ratio of 0.4, an aspect ratio of 4.0, and a modified NACA 0008-64 airfoil section. A 0.30c aileron (measured perpendicular to hinge line) was located between the 40-percent and 85-percent-semispan stations of the wing. The aileron was made integral with the wing by cutting grooves 0.03 inch wide along the 73-percent-chord line on the upper and lower surfaces of the wing. Aileron deflections were set by bending the metal along the grooves which were faired with wax. The model contained a duct with a static- and a total-pressure tube as shown in figure 1. A removable canopy was attached to the model. The tail deflection angle was changed by removing the complete empennage and adding another which had the horizontal tail constructed with the desired angle. A second model of the wing (with 0° dihedral angle) was used for the wing-alone tests.

The models were constructed at the Langley Laboratory and were of bismuth and tin poured around steel stiffening spars. The models were designed and the molds and steel parts of the models were made by the Consolidated Vultee Aircraft Corporation, San Diego, Calif.

The models were mounted on an electrical strain-gage balance which was wired to calibrated galvanometers in order to measure the aerodynamic forces and moments. The balance was mounted in a chamber within the bump, and the chamber was sealed except for a small rectangular hole through which an extension of the wing passed. In the wing-alone test this hole was covered by a $\frac{1}{32}$ -inch end plate located approximately 0.03 inch above the bump surface with the dimensions shown in figure 1.

Photographic records of the shock patterns over the model were obtained by directing a strong point light source in the model's plane of symmetry toward the model so as to cast the model and shock shadows on the opposite wall of the tunnel.

TESTS

The tests were conducted in the Langley high-speed 7- by 10-foot tunnel using an adaptation of the NACA wing-flow technique for obtaining transonic speeds. The technique used involves placing the model in the high-velocity flow field generated over the curved surface of a bump on the tunnel floor (reference 2). Typical contours of local Mach number in the vicinity of the model location on the bump with model removed are shown in figure 3. The long dashed lines near the wing root of the model in figure 3 indicate a local Mach number 5 percent below the maximum value and represent the estimated extent of the bump boundary layer. The effective test Mach number was obtained from contour charts similar to those presented in figure 3 by using the relationship $M = \frac{2}{5} \int_0^{b/2} cM_a dy$.

The variation of mean test Reynolds number with Mach number is shown in figure 4.

Force and moment data were obtained for the wing alone and the complete model configuration through a Mach number range of 0.60 to 1.16, and an angle-of-attack range of -21° to 26° . Aileron deflection ranged from -17.1° to 16.6° , and the tail deflection angles were -2° , -6.75° and -12.66° .

Flow Mach numbers in the jet-engine duct were determined from static- and total-pressure readings obtained by means of $\frac{1}{16}$ -inch-diameter tubes located as shown in figure 1. The duct was partially blocked near the exit by inserting machine screws through the cross section so that a duct Mach number corresponding to an inlet-velocity ratio of about 0.8 would be obtained at an airplane test Mach number of about 0.95 (estimated high-speed condition at 35,000 feet for the airplane). No attempt was made to fix the duct Mach number at other test Mach numbers. The velocity distribution across the duct was assumed such that the average velocity was 0.8 the velocity at the center. This type of distribution would be expected at the duct Reynolds numbers prevailing according to figure 88 of reference 3.

CORRECTIONS

The rolling effectiveness parameters presented herein represent the aerodynamic effects on a complete model produced by the deflection of the aileron on only one semispan of the complete wing. A reflection-plane correction has been applied to the rolling-moment data. The correction factor which was applied (measured rolling moment was reduced by 27.5 percent) was obtained from unpublished experimental low-speed data and theoretical considerations. Although the correction was based on low-speed considerations and is valid for the low Mach numbers only, it was believed that the results obtained by applying the correction would give a better representation of true conditions at high Mach numbers than uncorrected data.

The effect of the end plate on the wing-alone configuration was not subtracted from the data. However, it was estimated from unpublished data that the drag coefficient for the wing alone without end plate would be approximately 0.006 lower throughout the Mach number range.

No attempt has been made to evaluate the effects of either the chordwise or spanwise Mach number variation over the wing or the longitudinal Mach number variation from wing to tail shown in figure 3. Estimates indicated that the effects of model elasticity would generally be small; consequently no corrections for structural distortion were applied to the data.

RESULTS

The results of the transonic-bump investigation of the $\frac{1}{80}$ -scale model of the Skate 9 airplane are presented as follows:

	Figure
Longitudinal aerodynamic characteristics	5 and 6
Longitudinal-stability parameters	7
Tail incidence required for trim C_L	8
Tail incidence required for accelerated maneuvers	9
Aileron characteristics	10 and 11
Duct characteristics	12 and 13
Shock patterns	14

DISCUSSION

Longitudinal Stability

The pitching-moment-coefficient curves (fig. 5) indicate that the model had control-fixed static longitudinal stability throughout the Mach number and angle-of-attack ranges tested except for a region generally extending from a lift coefficient of about 0.4 to 0.8 at Mach numbers below 1.0. The change in slope of the pitching-moment-coefficient curves occurred at about the same lift coefficient where the lift curves broke from linearity.

The stability loss in the region noted, can be partially attributed to instability of the sweptback wing alone. Comparison of the lift data and rolling-moment data for zero aileron deflection (not presented herein) indicates that the instability resulted from loss of lift on the outboard portion of the span. Stall-control devices, of course, might eliminate the instability if it is still presented at full-scale Reynolds numbers. However, comparison of wing-alone and tail-off tests indicates that the hull also had a destabilizing effect at the higher lift coefficients. The loss in stability in the region noted was also more severe with the tail on than with tail off. Calculations have indicated that this was the region for the largest variation of downwash with angle of attack, $d\epsilon/d\alpha$.

At Mach number 1.0 and higher the unstable region in the pitching-moment-coefficient curve was generally eliminated. In a few instances a region of about neutral stability remained near maximum lift coefficient.

Similar pitching-moment-coefficient trends occurred for a wing of similar plan form in reference 4 where it was noted that the increased stability at the higher Mach numbers resulted from a Mach number increase rather than an increase in Reynolds number.

Figure 6 includes the variation of the pitching-moment coefficient with Mach number for various component parts of the model tested at angles of attack of 2° and 8° . At the low angle of attack there was generally little change in pitching-moment coefficient with Mach number regardless of configuration. At an angle of attack of 8° , however, a pronounced increase in negative pitching-moment coefficient occurred at Mach numbers between 0.9 and 1.0 which was most severe for the complete model and corresponded to an increment of approximately 4° negative control deflection for trim. This diving tendency corresponded to the reduction in instability at the high Mach numbers mentioned previously.

An indication of the increase of longitudinal stability of the airplane with Mach number at low lift coefficients is shown in figure 7. The aerodynamic-center position of the airplane as determined from the slopes of the pitching-moment-coefficient curve with lift coefficient $\partial C_m / \partial C_L$, at low lift coefficients and at a stabilizer angle of -6.75° increased gradually from 37 percent mean aerodynamic chord at a Mach number of 0.6 to 42 percent mean aerodynamic chord at Mach number 0.9 and then shifted rearward sharply with increasing Mach number to about 64 percent mean aerodynamic chord at a Mach number of 1.1. The aerodynamic-center position was moved rearward slightly by the addition of the hull to the wing alone above a Mach number of 0.8. The addition of the tail to the model caused the largest stability increase to the model in the range of Mach numbers above 0.97.

The lift-curve slope for the wing alone reached a maximum value of 0.076 at a Mach number of 0.89; the values agreed very well up to a Mach number of 0.90 with those predicted for the wing alone by theory of reference 5. The addition of the hull which blended into the wing resulted in a lift-curve slope that was somewhat higher than that of the wing alone throughout the entire Mach number range.

Longitudinal Control

The tail deflection angle required for trim varied only slightly with Mach number in the low lift-coefficient range up to a Mach number of about 0.95 (fig. 8). Above a Mach number of 0.95 the tail angle required for trim generally increased negatively with Mach numbers. At lift coefficients beyond about 0.45 for the lower Mach numbers a reversal occurred in the elevator trim-lift-coefficient curves which resulted largely from the instability of the swept wing and fuselage mentioned previously. The tail effectiveness $\partial C_m / \partial i_t$ increased gradually up to a Mach number of about 0.95 (fig. 7) and then decreased slightly with Mach number. As shown in figure 9, the estimated tail deflection angle required for steady flight and accelerated maneuvers generally should not vary greatly with Mach number for the Skate airplane at sea level with a wing loading of 42.5 pounds per square foot. For accelerated maneuvers at altitude the variation of tail angle with Mach number was erratic because of the reversal in the $C_{L_{trim}}$ curves above a lift coefficient of 0.45 (fig. 8).

Lateral Control

The effect of aileron deflection on the aerodynamic characteristics of the model is presented in figures 10 and 11. In general the rolling-moment coefficient varied approximately linearly with aileron deflection in the range of deflections tested (-17.1° to 16.6°). At low angles of attack unfavorable yawing-moment coefficients resulting from positive

aileron deflections were about equal to favorable yawing-moment coefficients resulting from negative deflections. For the complete wing at low angles of attack the yaw due to ailerons should therefore be small. In general as the angle of attack was increased adverse yaw resulted over the complete deflection range. As shown in figure 11, a marked decrease occurred in the rolling effectiveness $C_{l\delta}$ between the Mach numbers of 0.85 and 0.95 over the complete angle of attack range except for an angle of 16° where a steady rise occurred up to a Mach number of about 1.05. The theoretical value of 0.0013 for the rolling effectiveness at low Mach numbers (reference 6) was found to be in fair agreement with the test data.

Drag Characteristics

From figures 5 and 6 it can be seen that at low lift coefficients there was generally a slight increase in the drag coefficient up to a Mach number of 0.90 for the complete model and 0.95 for the wing alone where a sudden increase occurred. The blended hull, tested in reference 1, also had a drag break occurring earlier than the wing alone. The drag coefficient rise tended to level off after a Mach number of 1.05 and generally decreased as the Mach number was increased. At the higher angle of attack (8°) a drag coefficient increase with Mach number started at the lowest Mach number tested.

At angles of attack of 2° and 8° removing the canopy generally had a negligible effect on the drag coefficient or caused a small drag-coefficient decrease.

Duct Characteristics

The variation of the Mach number in the rear part of the jet-engine duct with angle of attack of the model and model Mach number is shown in figures 12 and 13. For the range investigated, angle-of-attack and Mach number changes caused no sudden Mach number losses in the duct and the canopy had only a small effect on the duct Mach number.

Shock Patterns

Typical photographs of the shock patterns over the model presented in figure 14 show that at an angle of attack of 0° and at a Mach number of 1.0 shock lines occurred somewhere in the vicinity of the duct inlet and at the trailing edge of the wing tip. However, no abrupt flow losses occurred in the jet-engine duct at this Mach number according to figure 13. As the Mach number increased a well-defined shock line appeared at the tail section approximately parallel to the one at the wing tip.

The two lines at the wing tip and at the tip of the tail, approximately parallel to the plane of symmetry, which appeared as the angle of attack was increased can probably be attributed to tip vortices.

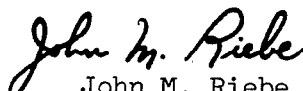
CONCLUSIONS


The results of tests made on the transonic bump in the Langley high-speed 7- by 10-foot tunnel of a $\frac{1}{80}$ -scale model of the Consolidated Vultee Skate 9 seaplane indicate the following conclusions:

1. At moderate lift coefficients and below a Mach number of 1.0 the model was statically unstable longitudinally as a result of loss of lift over the outboard portion of the wing and because of a fuselage destabilizing effect.
2. The static longitudinal stability of the model at low lift coefficients increased with Mach number corresponding to a shift in aerodynamic center from 37 percent mean aerodynamic chord at a Mach number of 0.60 to 64 percent at a Mach number of 1.10.
3. Estimates indicate that the tail deflection angle required for steady flight and accelerated maneuvers of the Skate 9 airplane probably would not vary greatly with Mach number at sea level; for accelerated maneuvers at altitude the tail deflection angle would probably vary erratically with Mach number.
4. The rolling-moment coefficient varied approximately linearly with aileron deflection angle and the rolling-moment effectiveness agreed well with theory.
5. At low lift coefficients the drag rise occurred at Mach numbers of 0.95 and 0.90 for the wing alone and complete model respectively.


6. For the range of angles of attack and Mach numbers investigated no sudden Mach number losses occurred in the jet-engine duct.

Langley Aeronautical Laboratory
National Advisory Committee for Aeronautics
Langley Field, Va.


John M. Riebe
Aeronautical Research Scientist


Richard G. MacLeod
Aeronautical Research Scientist

Approved:


for Thomas A. Harris
Chief of Stability Research Division

GMF

REFERENCES

1. Riebe, John M., and MacLeod, Richard G.: Preliminary Wind-Tunnel Investigation at High-Subsonic Speeds of Planing-Tail, Blended, and Airfoil-Forebody Swept Hulls. NACA RM L9D01, 1949.
2. Schneider, Leslie E., and Ziff, Howard L.: Preliminary Investigation of Spoiler Lateral Control on a 42° Sweptback Wing at Transonic Speeds. NACA RM L7F19, 1947.
3. Vennard, John K.: Elementary Fluid Mechanics. Second ed., John Wiley & Sons, Inc., 1947.
4. Turner, Thomas R.: Maximum-Lift Investigation at Mach Numbers from 0.05 to 1.20 of a Wing with Leading Edge Swept Back 42° . NACA RM L9K03, 1950.
5. DeYoung, John: Theoretical Additional Span Loading Characteristics of Wings with Arbitrary Sweep, Aspect Ratio, and Taper Ratio. NACA TN 1491, 1947.
6. Lowry, John G., and Schneider, Leslie E.: Estimation of Effectiveness of Flap-Type Controls on Sweptback Wings. NACA TN 1674, 1948.

TABLE I

CHARACTERISTICS OF $\frac{1}{80}$ -SCALE CONSOLIDATED VULTEE SKATE 9 MODEL

[All dimensions are for a complete model]

Wing:

Area, square feet	0.158
Span, feet	0.797
Chord (root), feet	0.284
Chord (tip), feet	0.113
Aspect ratio	4.01
Taper ratio	0.396
Mean aerodynamic chord, feet	0.211
Incidence, degrees	2
Dihedral, degrees	2.55
Sweepback at 0.25c, degrees	40
Airfoil section	Modified NACA 0008-64

Horizontal tail:

Area, square feet	0.0237
Span, feet	0.307
Chord (root), feet	0.116
Chord (tip), feet	0.039
Aspect ratio	4.0
Taper ratio	0.333
Mean aerodynamic chord, feet	0.085
0.25 mean aerodynamic chord of wing to 0.25 mean aerodynamic chord of tail	0.478
Dihedral, degrees	5
Sweepback at 0.25c, degrees	40
Airfoil section	Modified NACA 0007-64

Hull:

Length, feet	0.913
Height (to canopy top), feet	0.122
Minimum dead-rise angle, degrees	32
Station 0 to leading edge of mean aerodynamic chord, feet	0.403


 NACA

TABLE I

CHARACTERISTICS OF $\frac{1}{80}$ -SCALE CONSOLIDATED VULTEE SKATE 9 MODEL - Concluded

Aileron:

Area (one aileron), square feet	0.0085
Span (along hinge line), feet	0.207
Chord (perpendicular to hinge line), percent	30.4
Chord (parallel to center line), percent	27.0
Span perpendicular to center line at hinge line, feet	0.174
Outboard station	$0.85\frac{b}{2}$
Inboard station	$0.40\frac{b}{2}$

Vertical tail:

Area square feet	0.0228
Height, feet	0.156
Chord (root), feet	0.225
Chord (tip), feet	0.067
Airfoil section (root)	NACA 64(112)-013
Airfoil section (tip)	Modified NACA 64-009
Tail height above base line, feet	0.240
Sweepback at $0.25\bar{c}$, degrees	53
Aspect ratio	1.07
Taper ratio	0.296

Duct dimensions (one duct):

Duct inlet area, square inches	0.090
Duct maximum area, square inches	0.159


 NACA

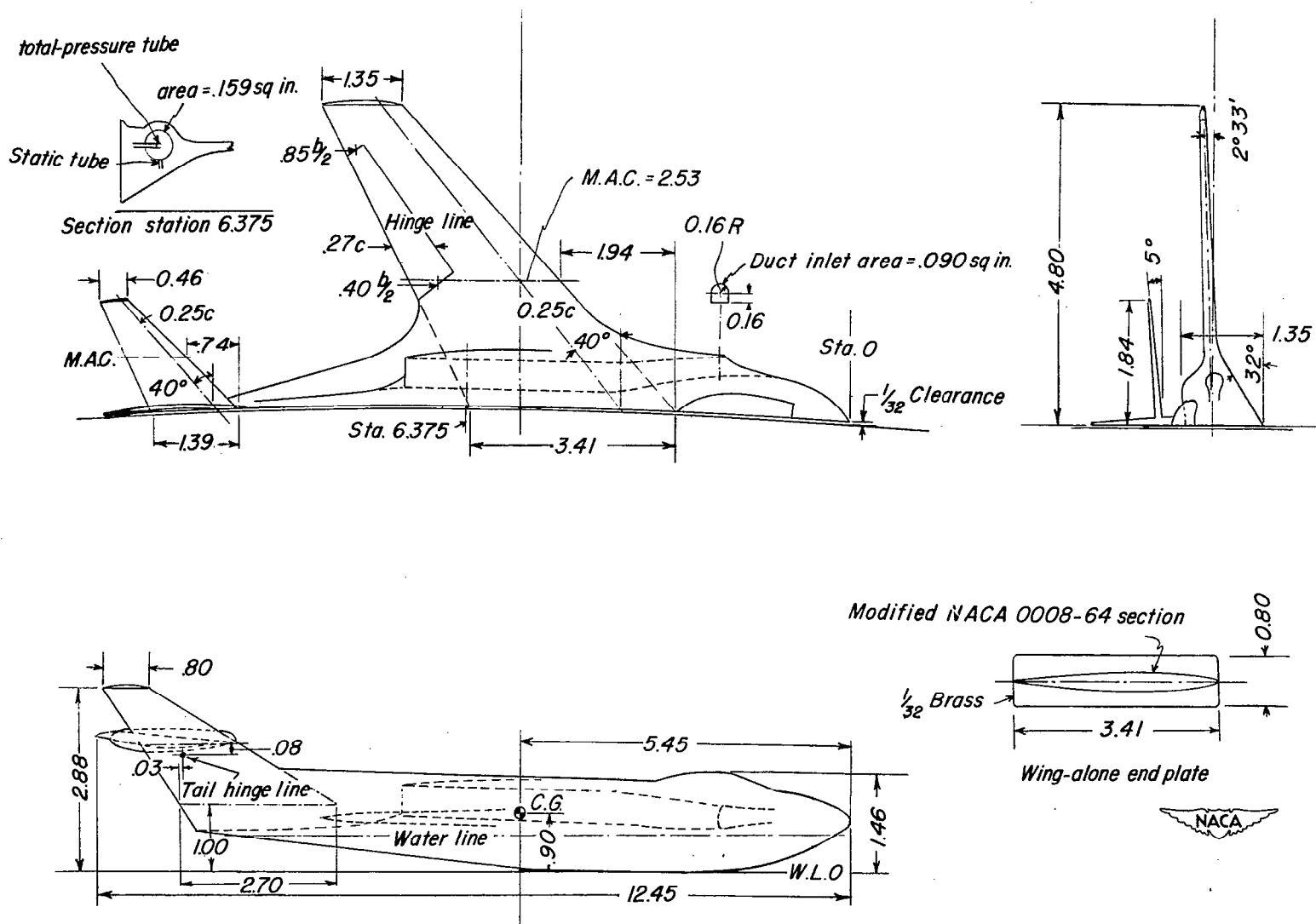
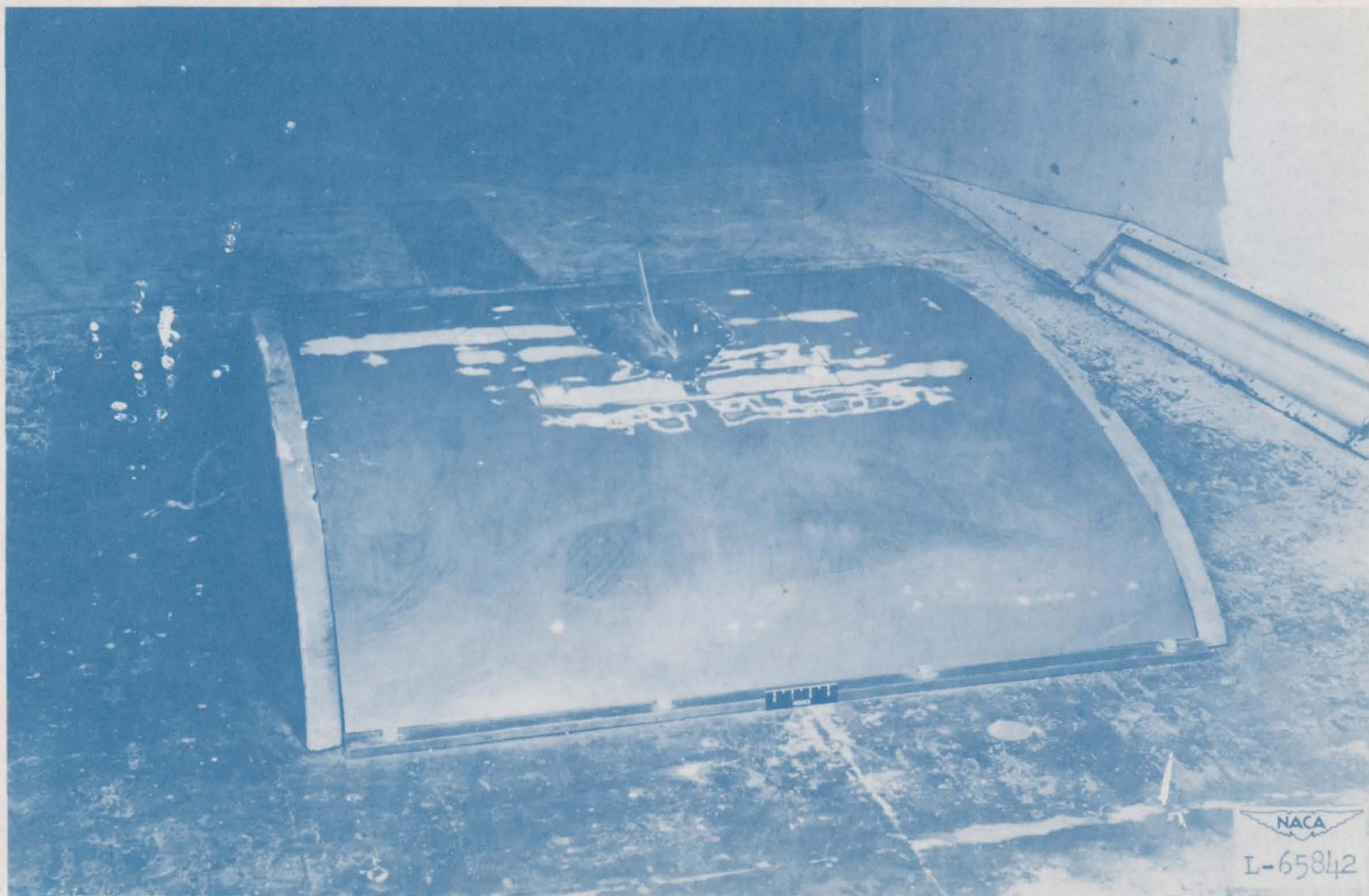
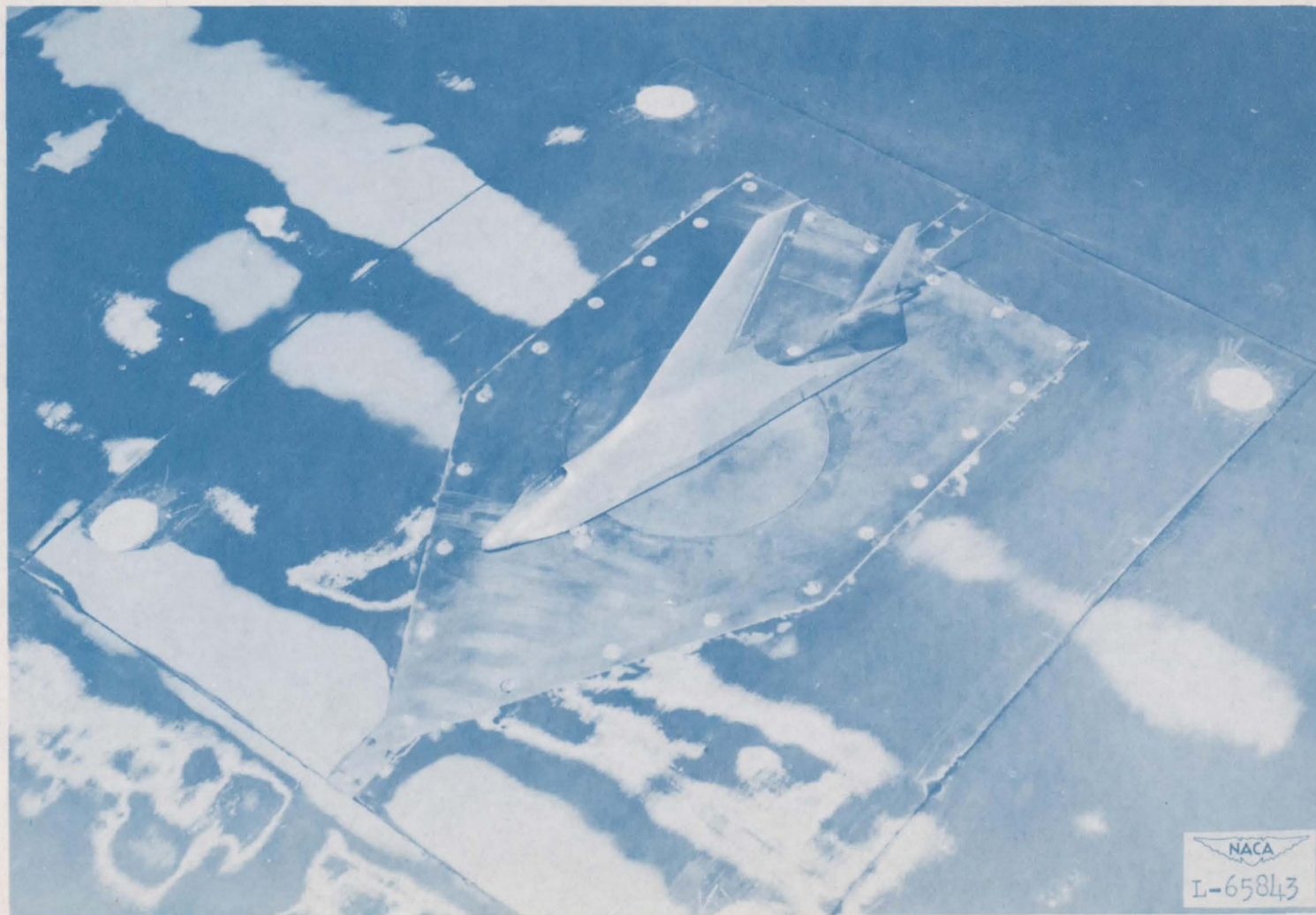


Figure 1.- General arrangement of the $\frac{1}{80}$ -scale model of the Convair Skate 9 airplane. All dimensions are in inches.



(a) $\alpha = 0^\circ$.

Figure 2.- View of test model in position on transonic bump.



(b) $\alpha = 10^\circ$.

Figure 2.- Concluded.

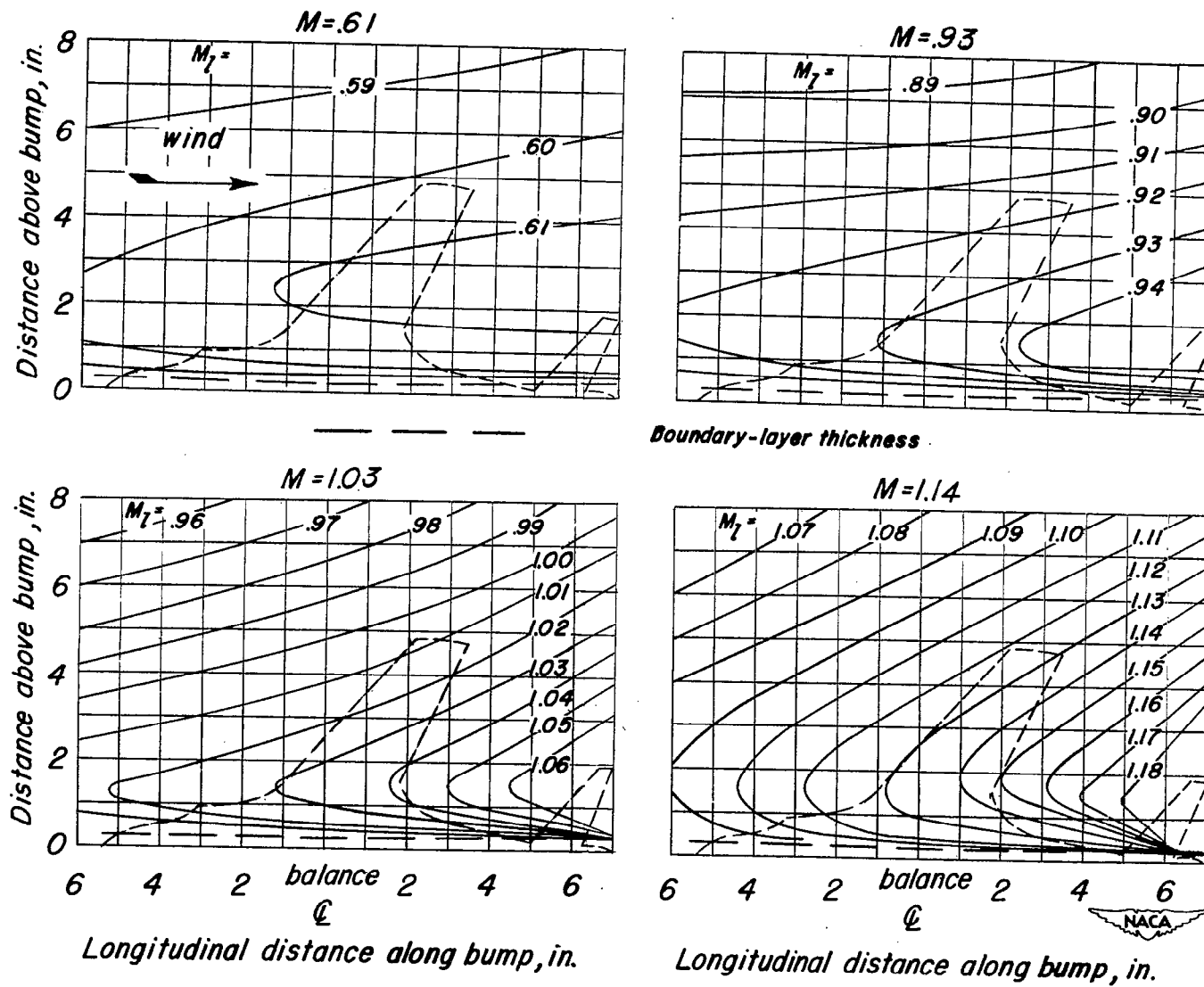
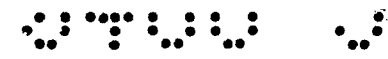


Figure 3.- Typical Mach number contour over transonic bump in region of model location.

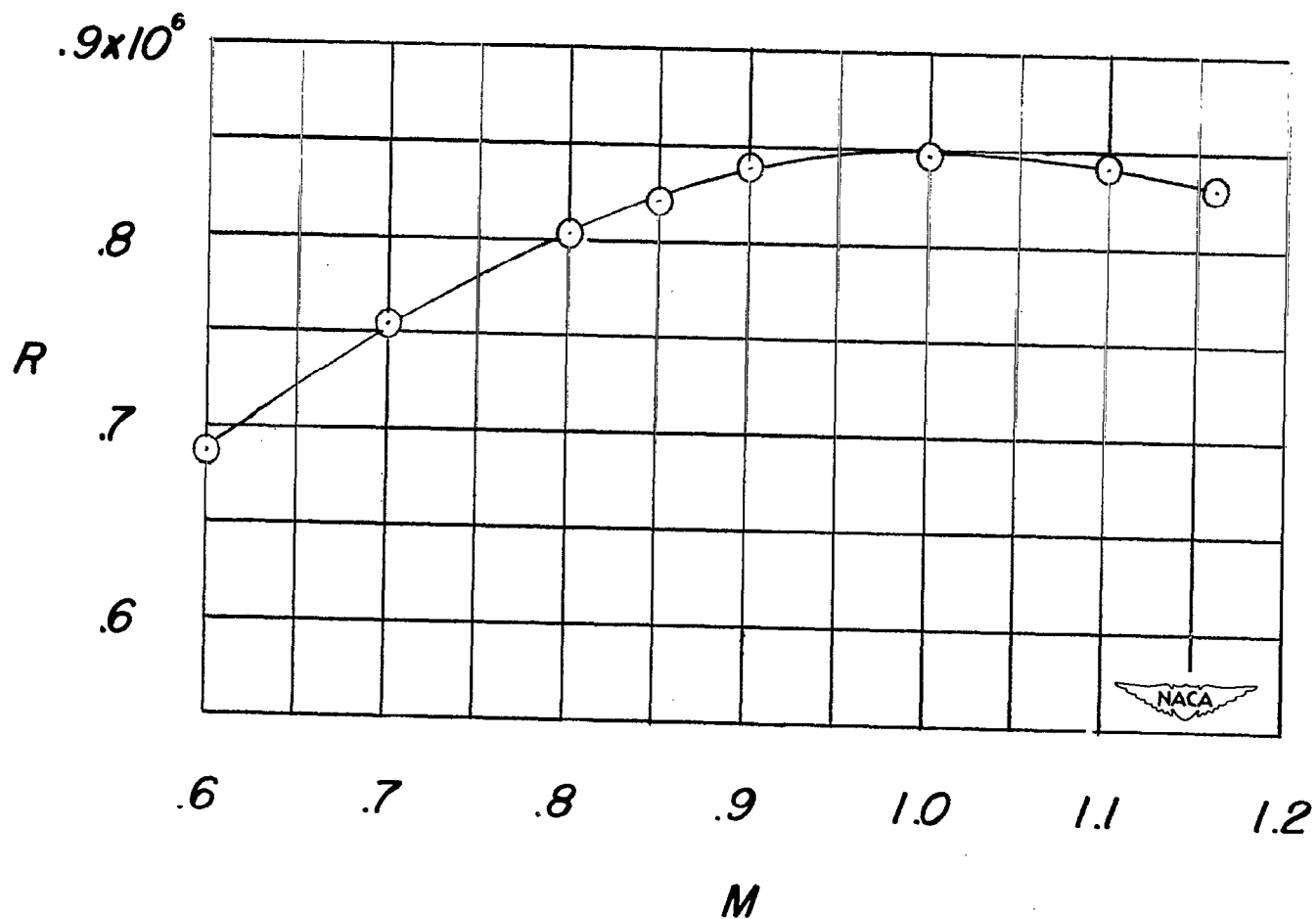


Figure 4.- Variation of test Reynolds number with Mach number for the test model.

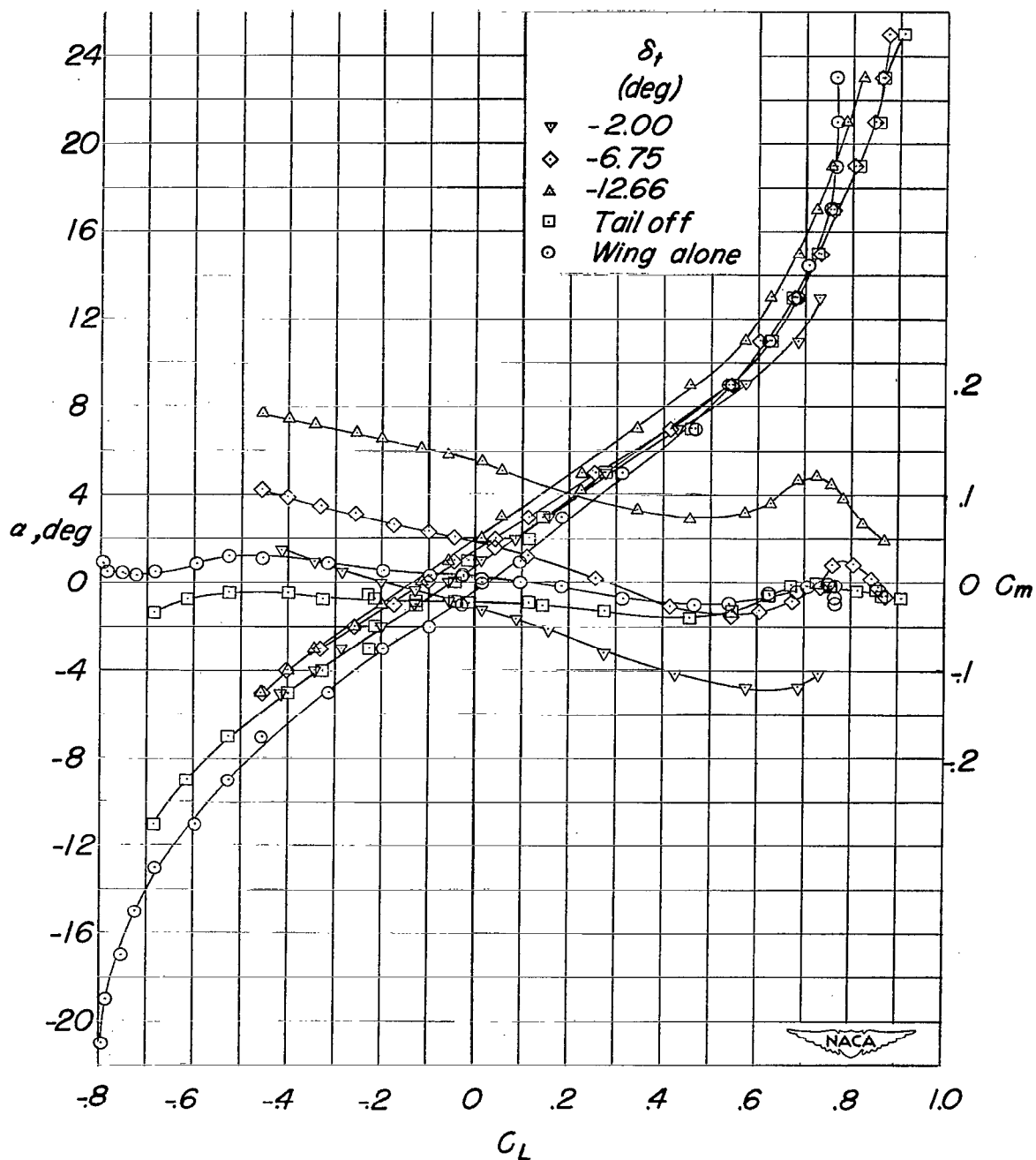
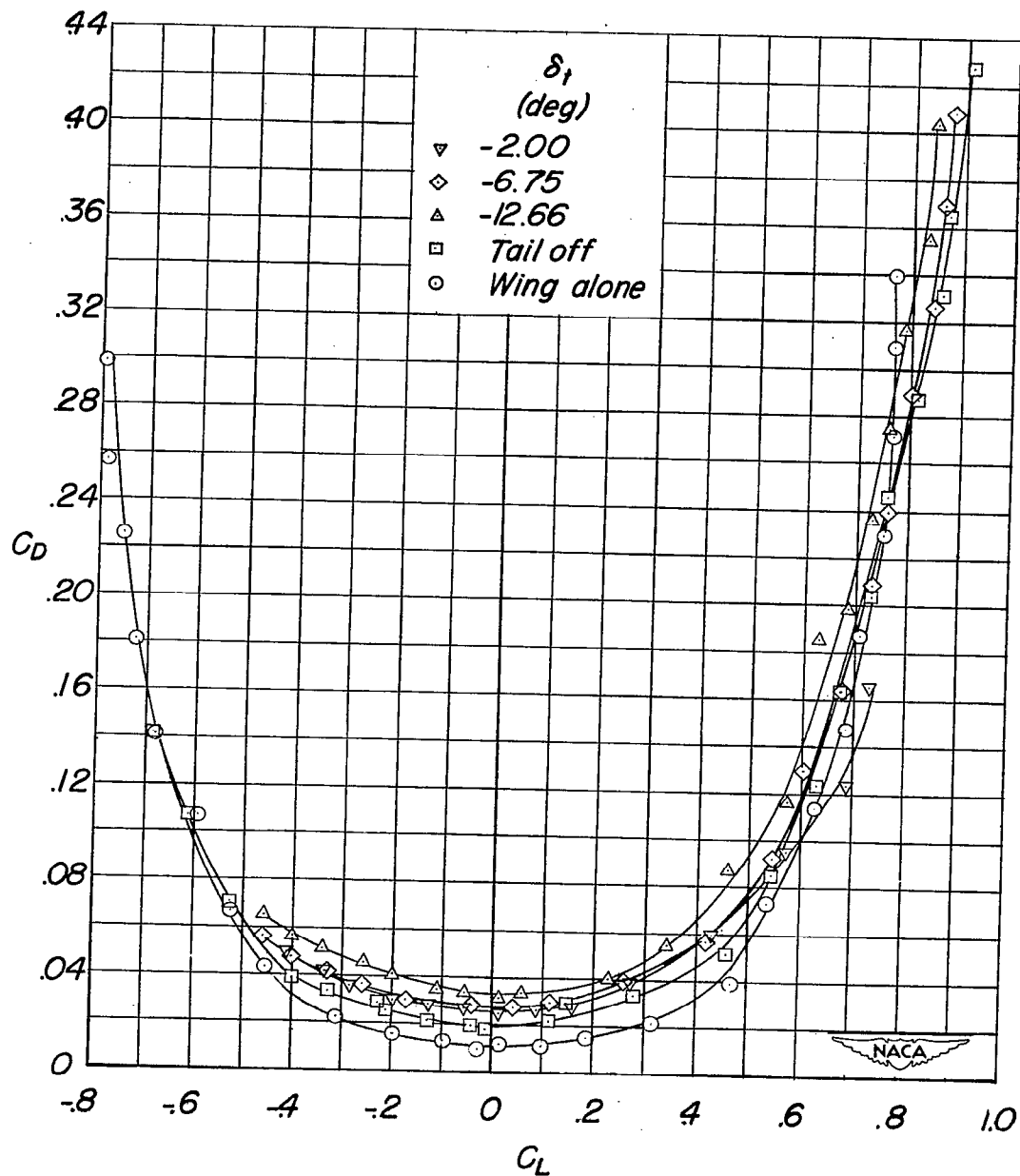
(a) $M = 0.60$.

Figure 5.- The longitudinal characteristics of the test model.



(a) $M = 0.60$ - Concluded.

Figure 5.- Continued.

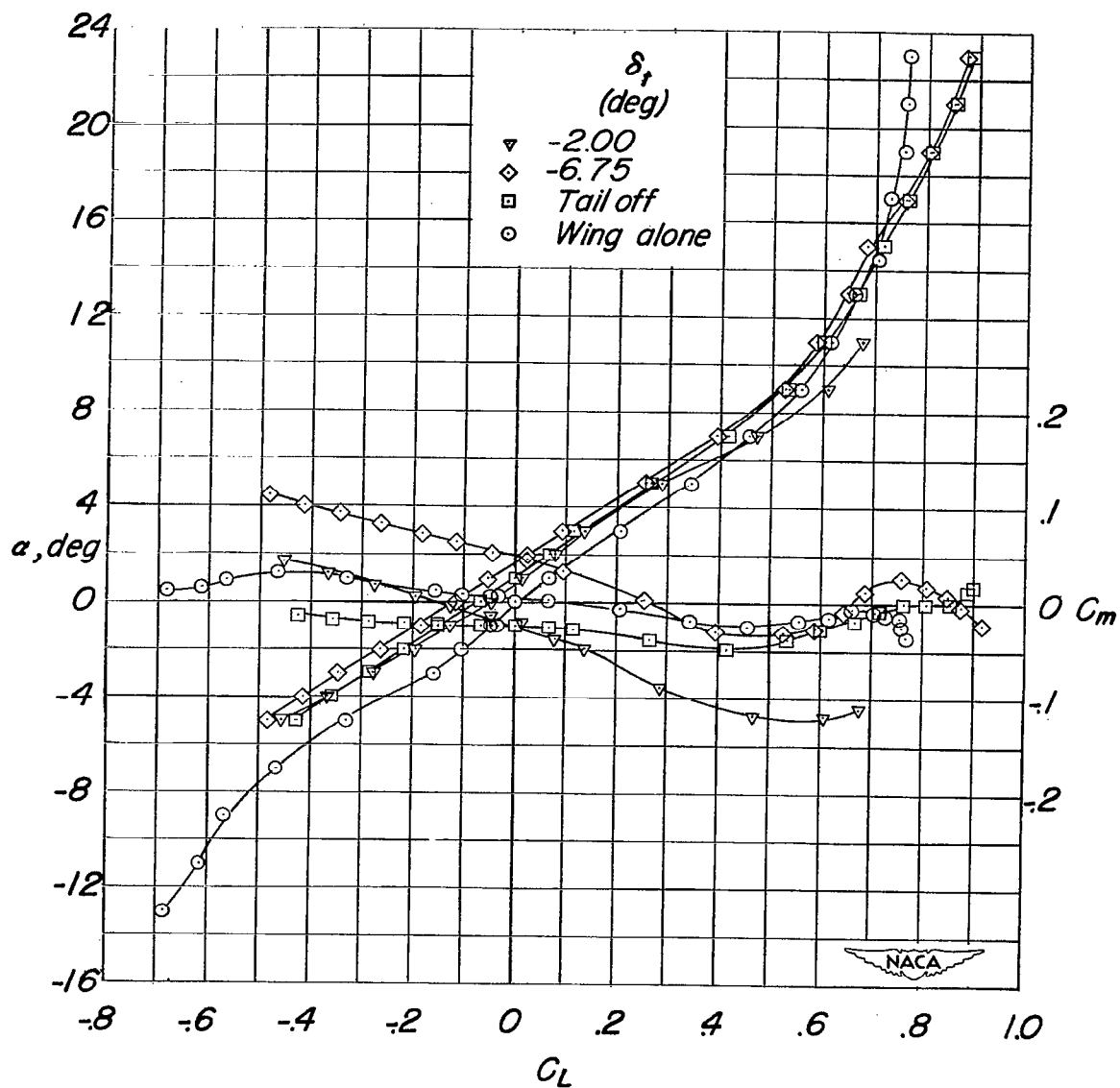
(b) $M = 0.70$.

Figure 5.- Continued.

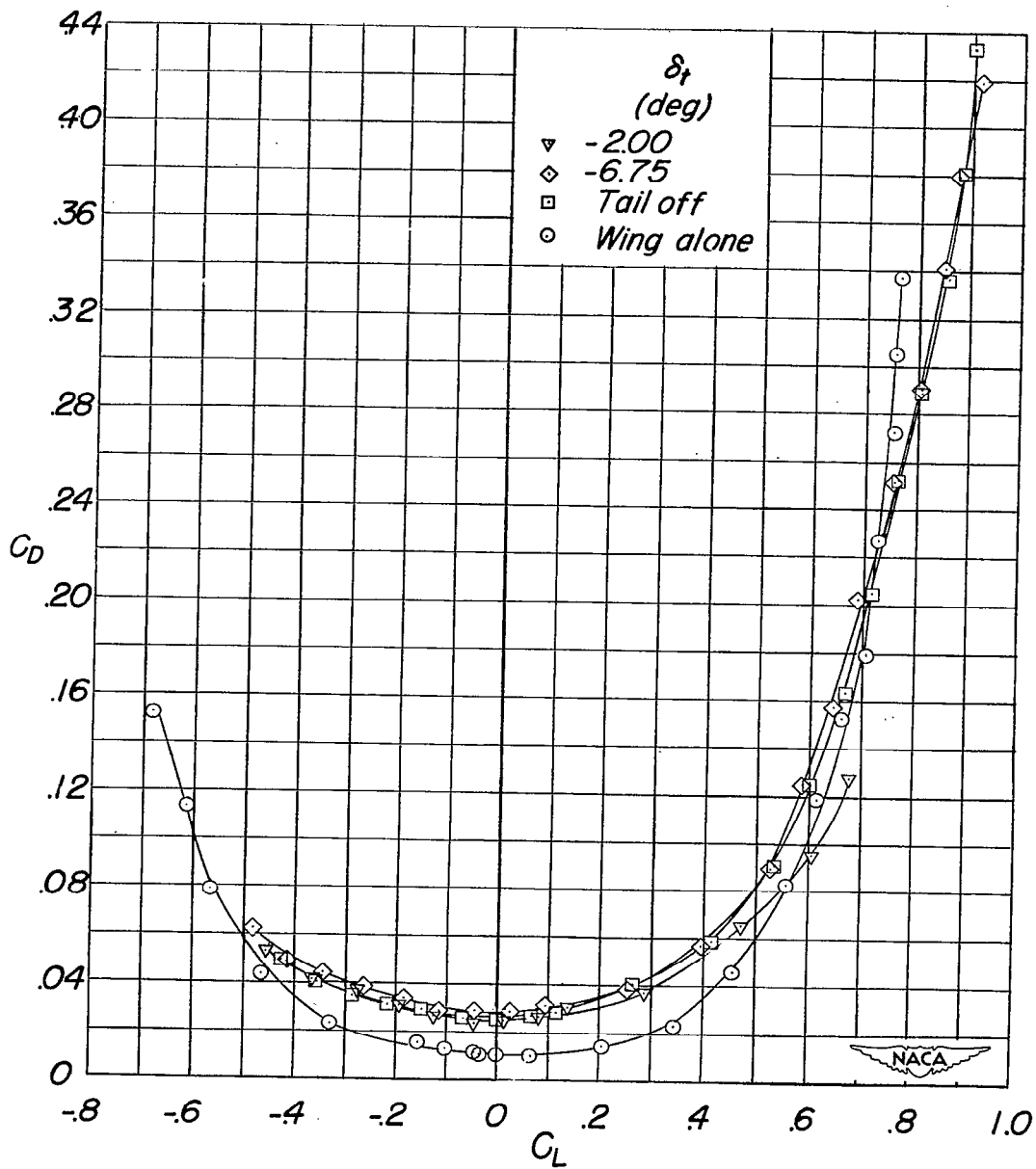
~~CONFIDENTIAL~~(b) $M = 0.70$ - Concluded.

Figure 5.- Continued.

~~CONFIDENTIAL~~

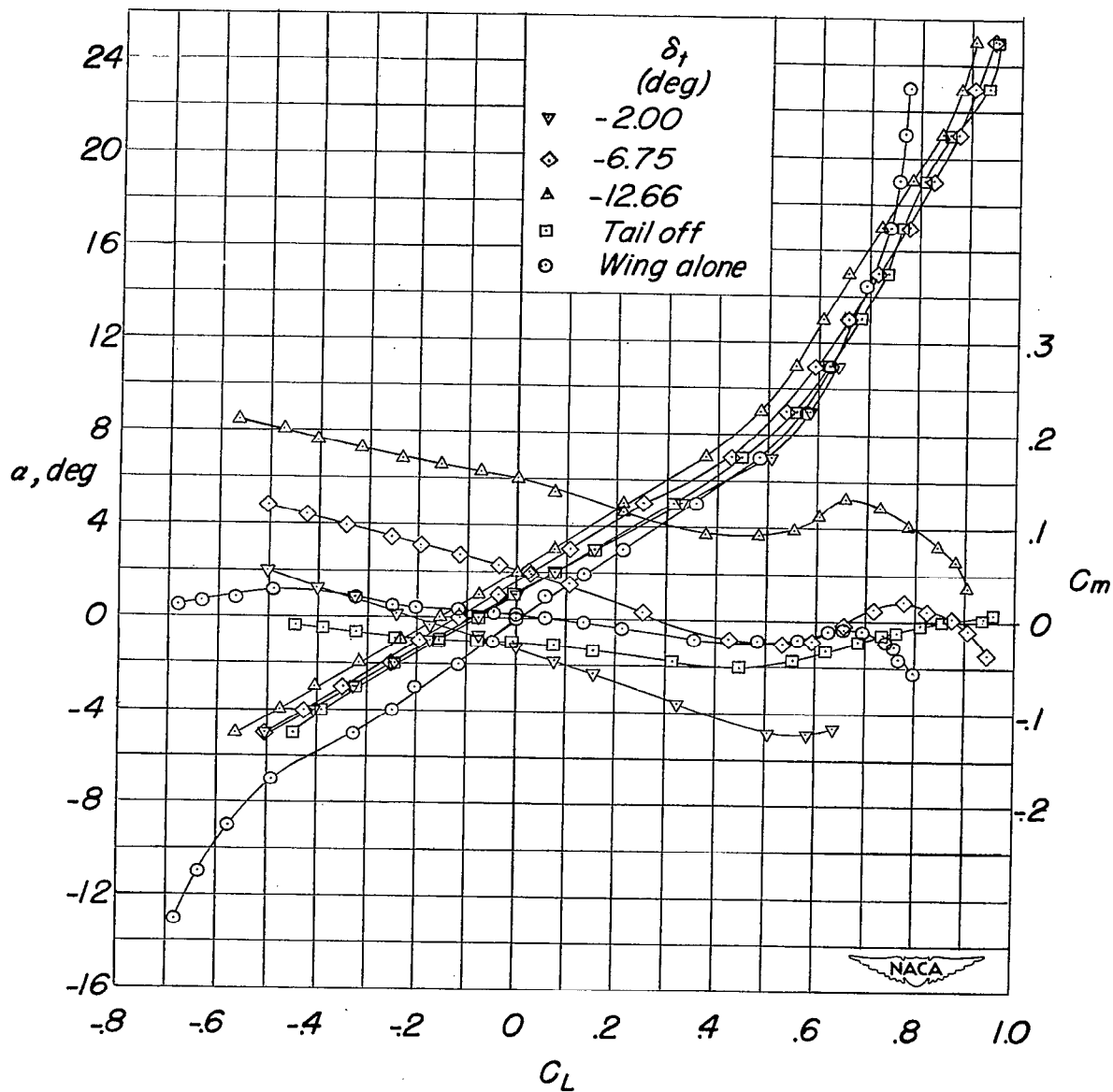
~~CONFIDENTIAL~~(c) $M = 0.80$.

Figure 5.- Continued.

~~CONFIDENTIAL~~

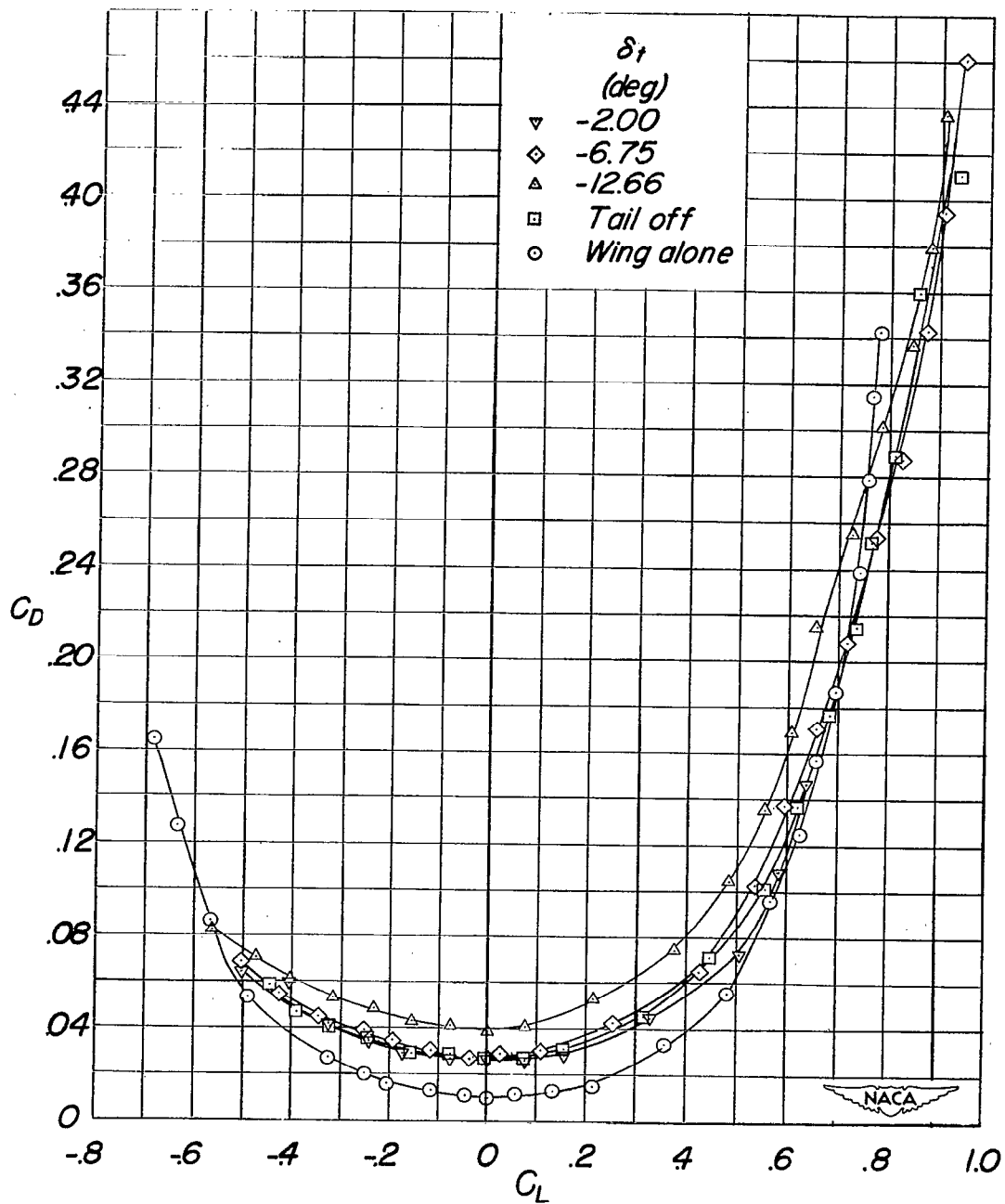
~~CONFIDENTIAL~~(c) $M = 0.80$ - Concluded.

Figure 5.- Continued.

~~CONFIDENTIAL~~

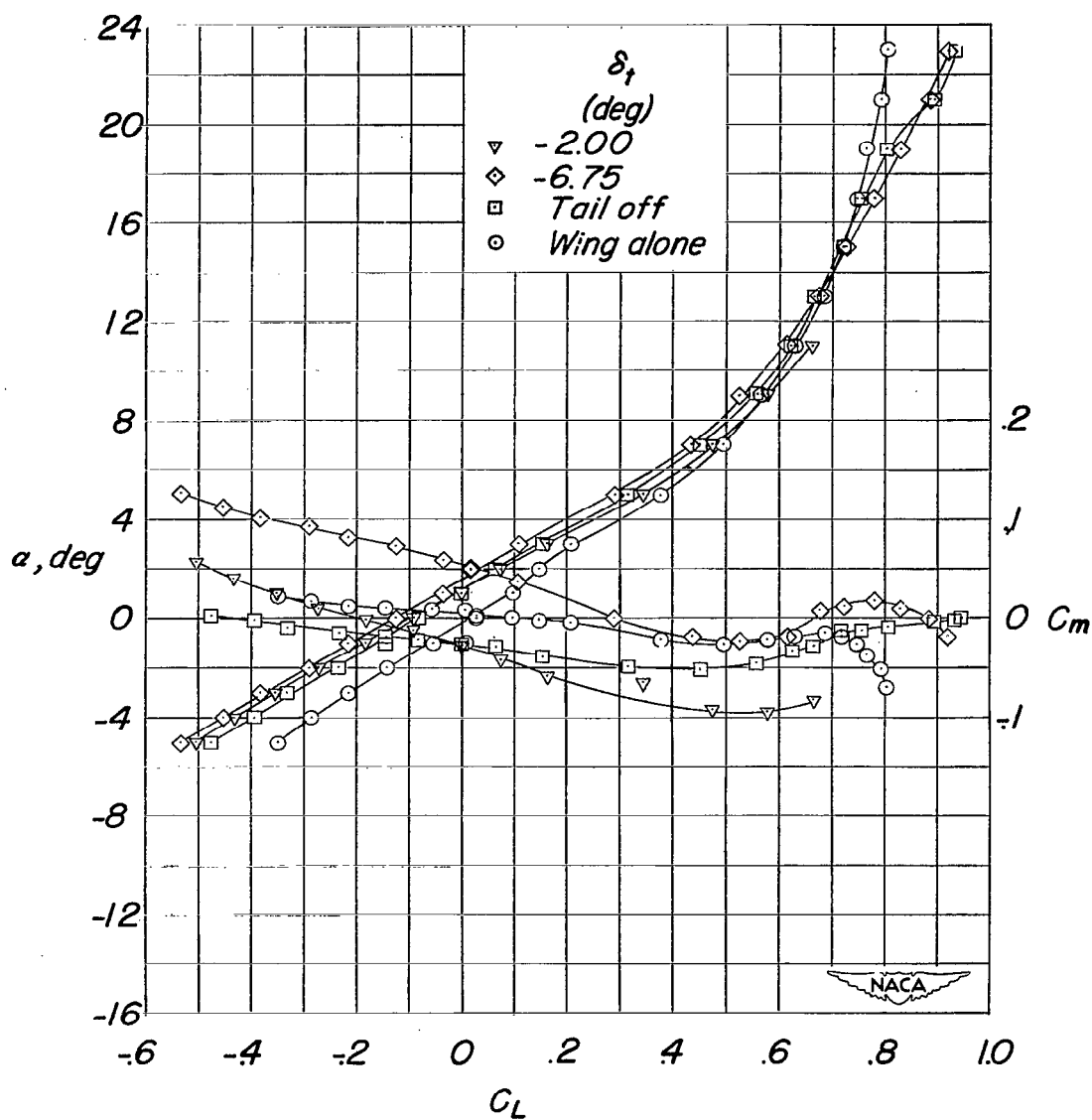
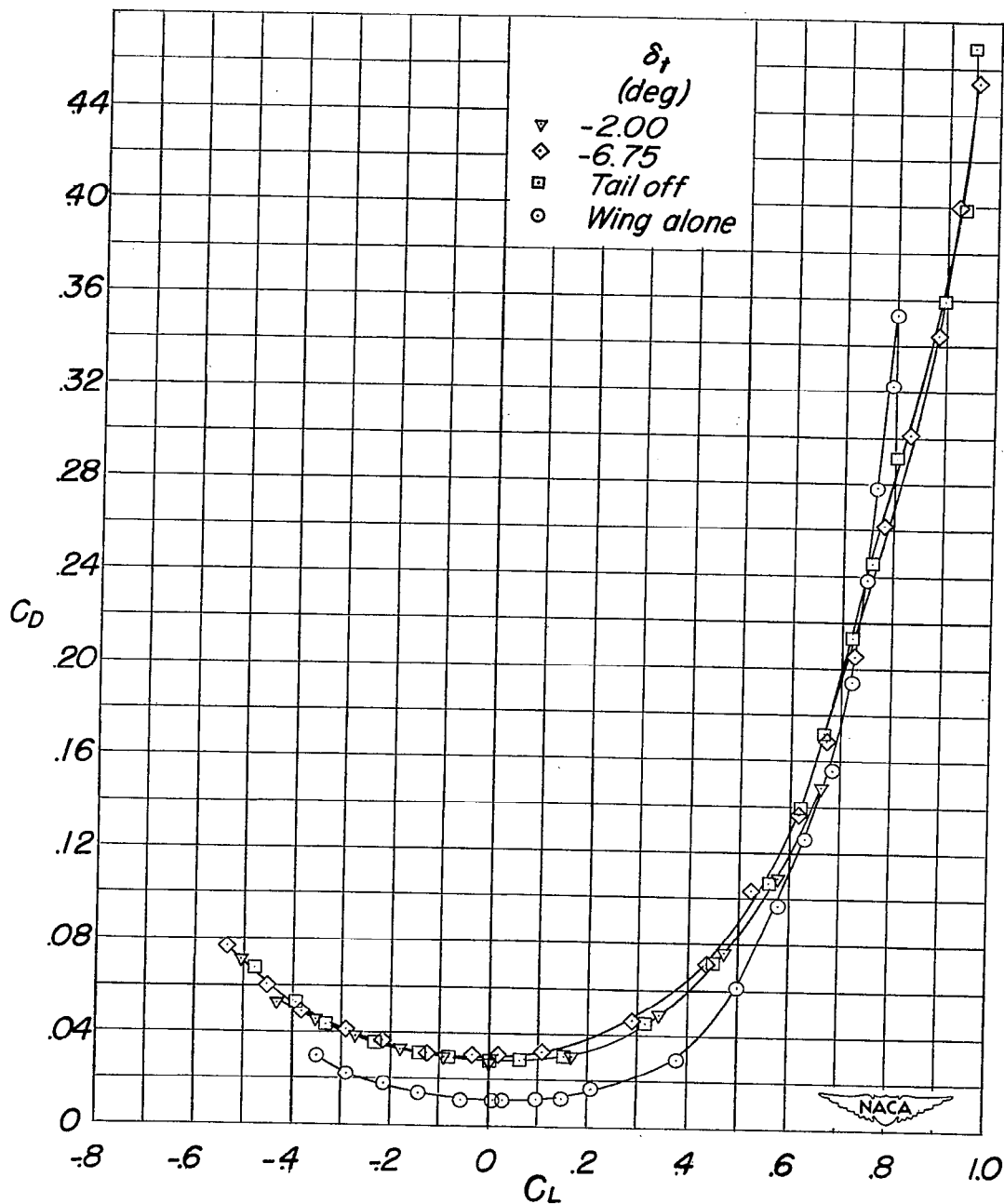
~~CONFIDENTIAL~~(d) $M = 0.85$.

Figure 5.- Continued.

~~CONFIDENTIAL~~



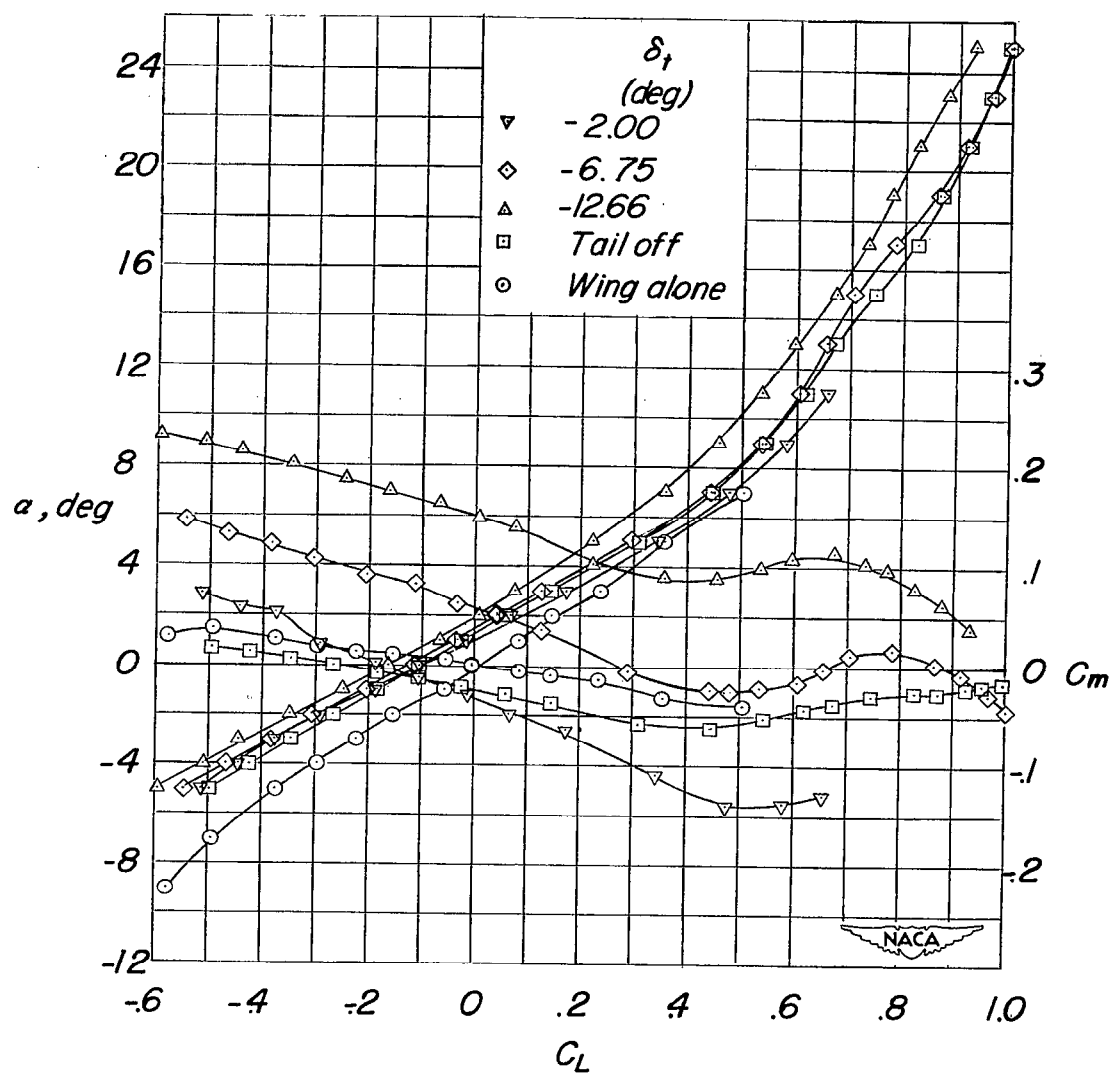
(e) $M = 0.90$.

Figure 5.- Continued.

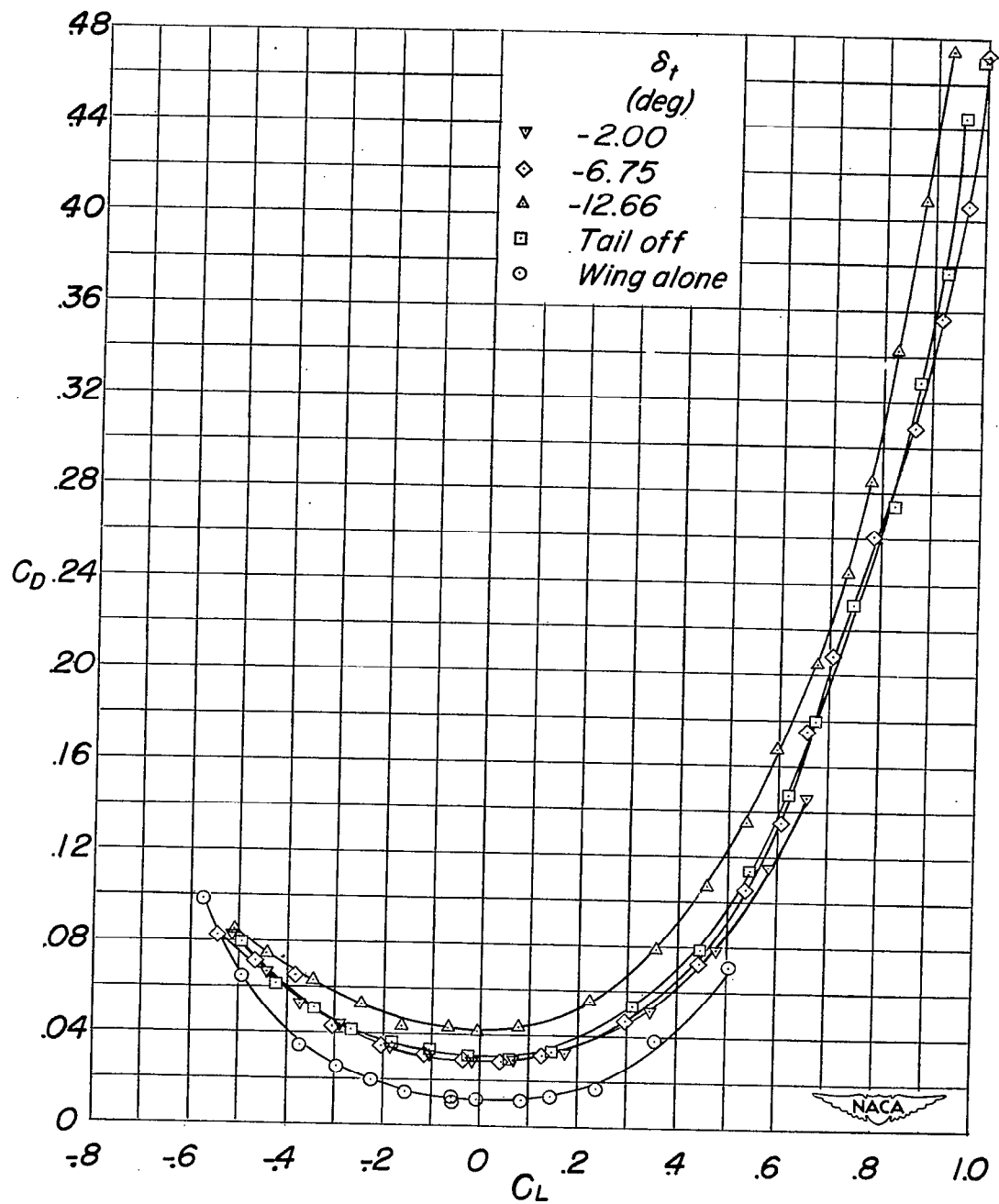
~~CONFIDENTIAL~~(e) $M = 0.90$ - Concluded.

Figure 5.- Continued.

~~CONFIDENTIAL~~

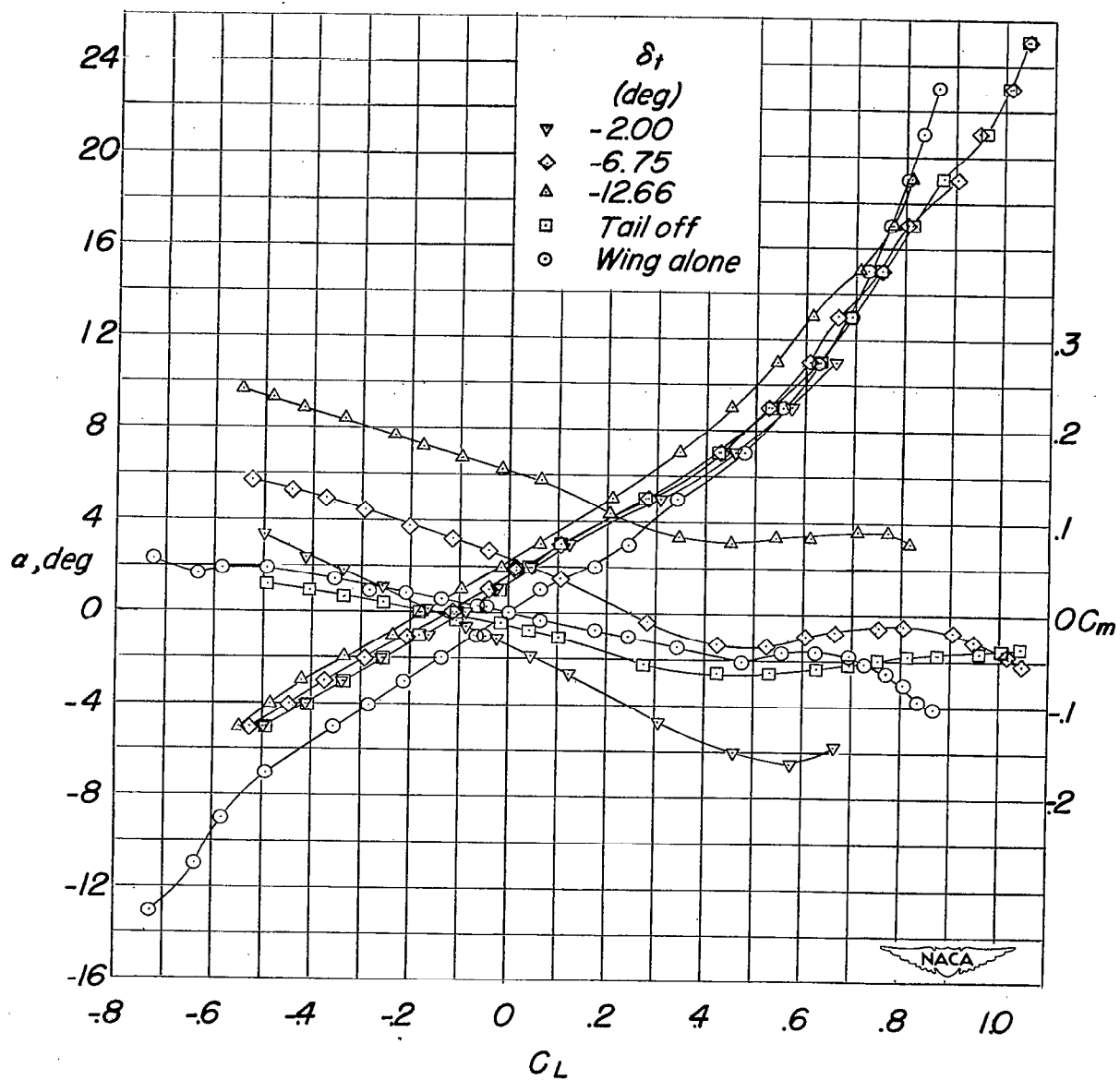
~~CONFIDENTIAL~~(f) $M = 0.95$.

Figure 5.- Continued.

~~CONFIDENTIAL~~

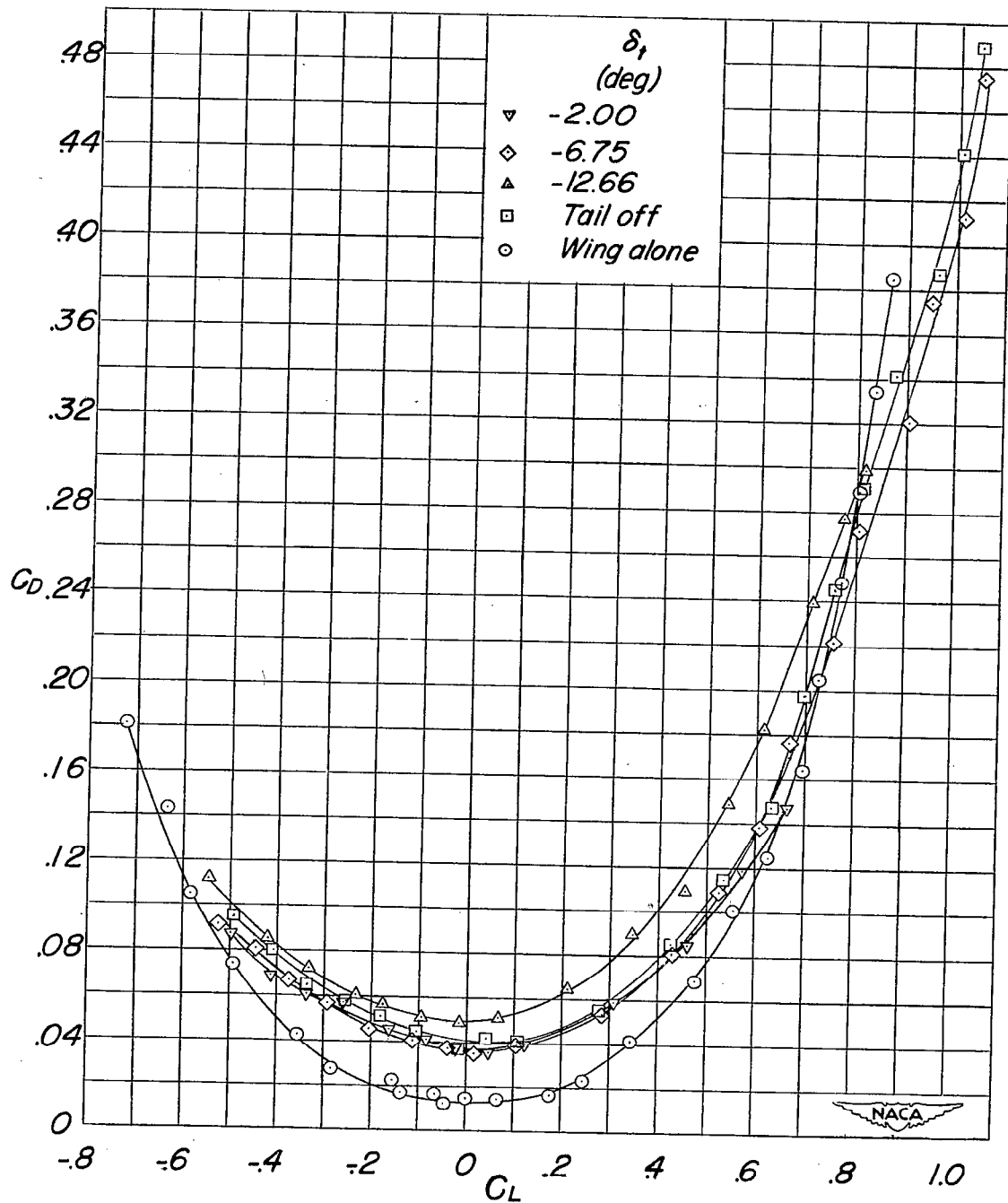
~~CONFIDENTIAL~~(f) $M = 0.95$ - Concluded.

Figure 5.- Continued.

~~CONFIDENTIAL~~

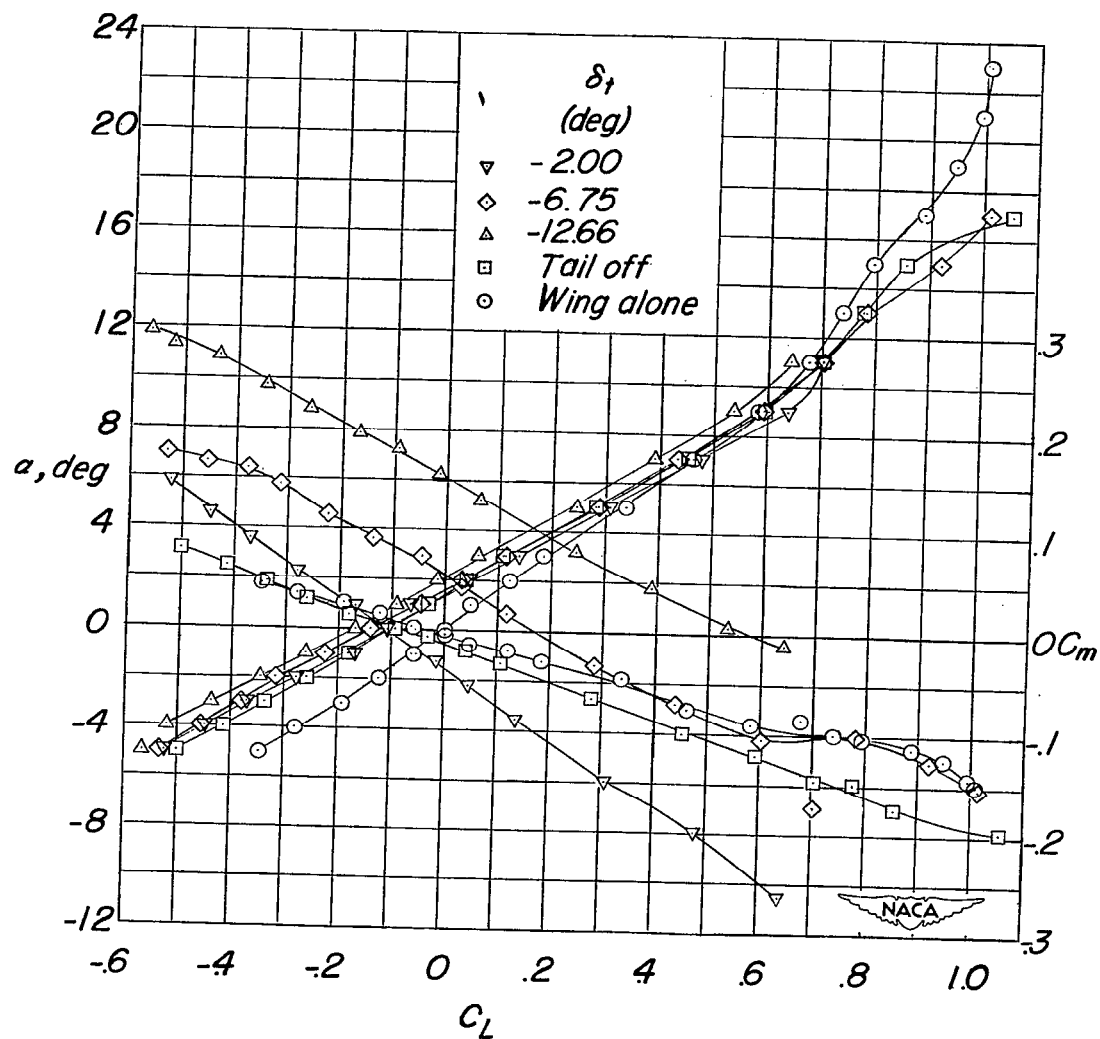
(g) $M = 1.00$.

Figure 5.- Continued.

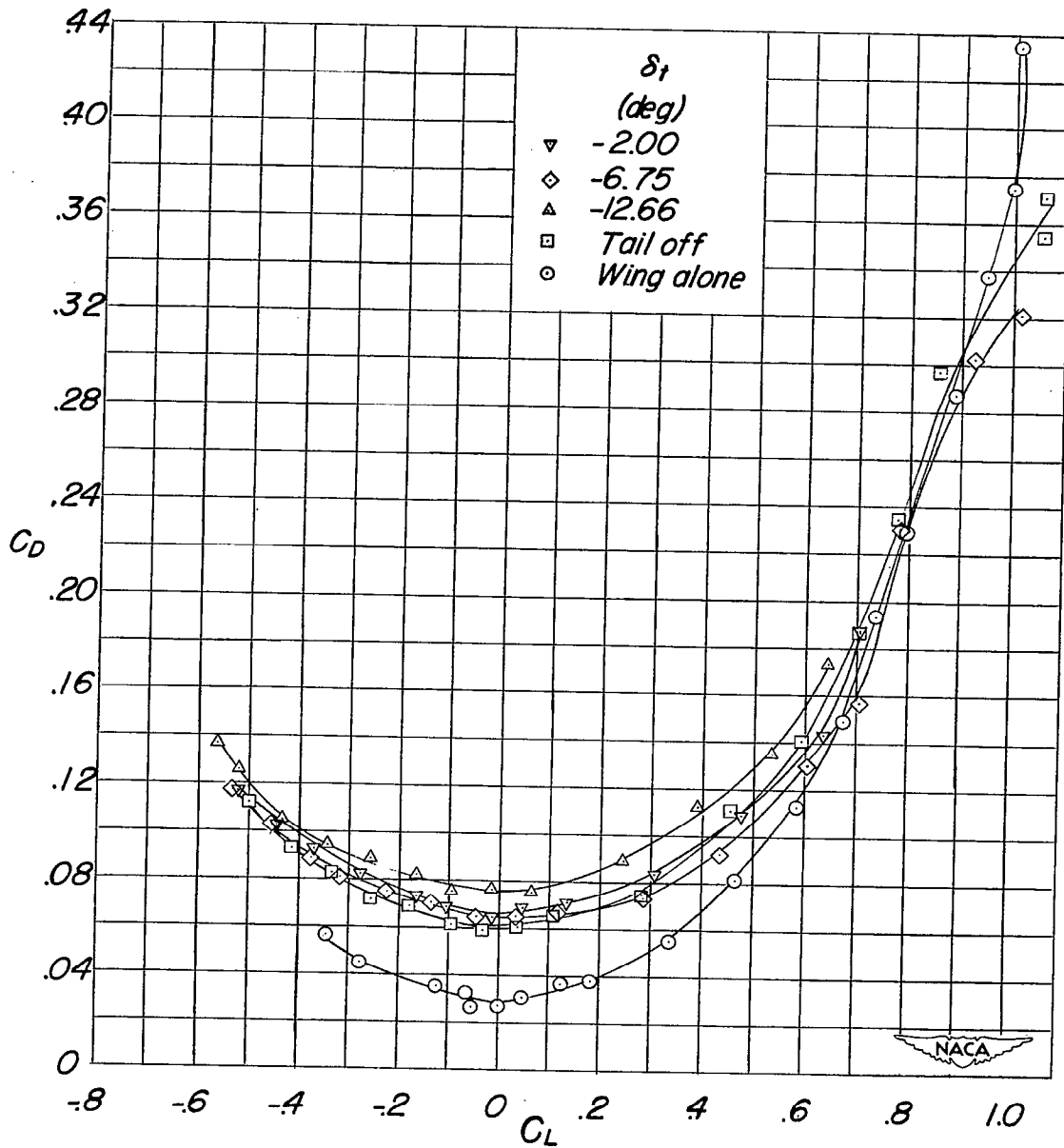
~~CONFIDENTIAL~~(g) $M = 1.00$ - Concluded.

Figure 5.- Continued.

~~CONFIDENTIAL~~

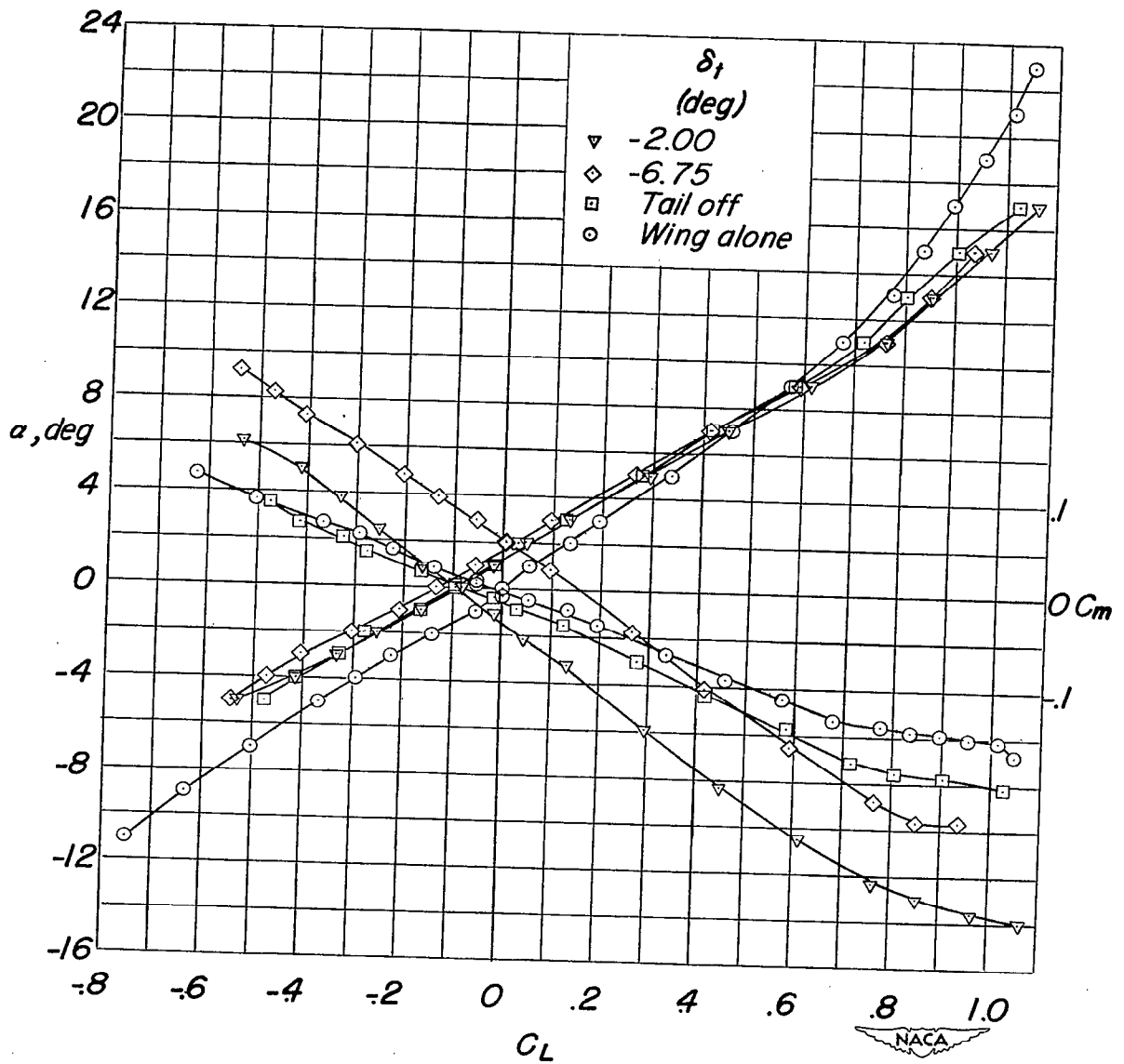
~~CONFIDENTIAL~~(h) $M = 1.05$.

Figure 5.- Continued.

~~CONFIDENTIAL~~

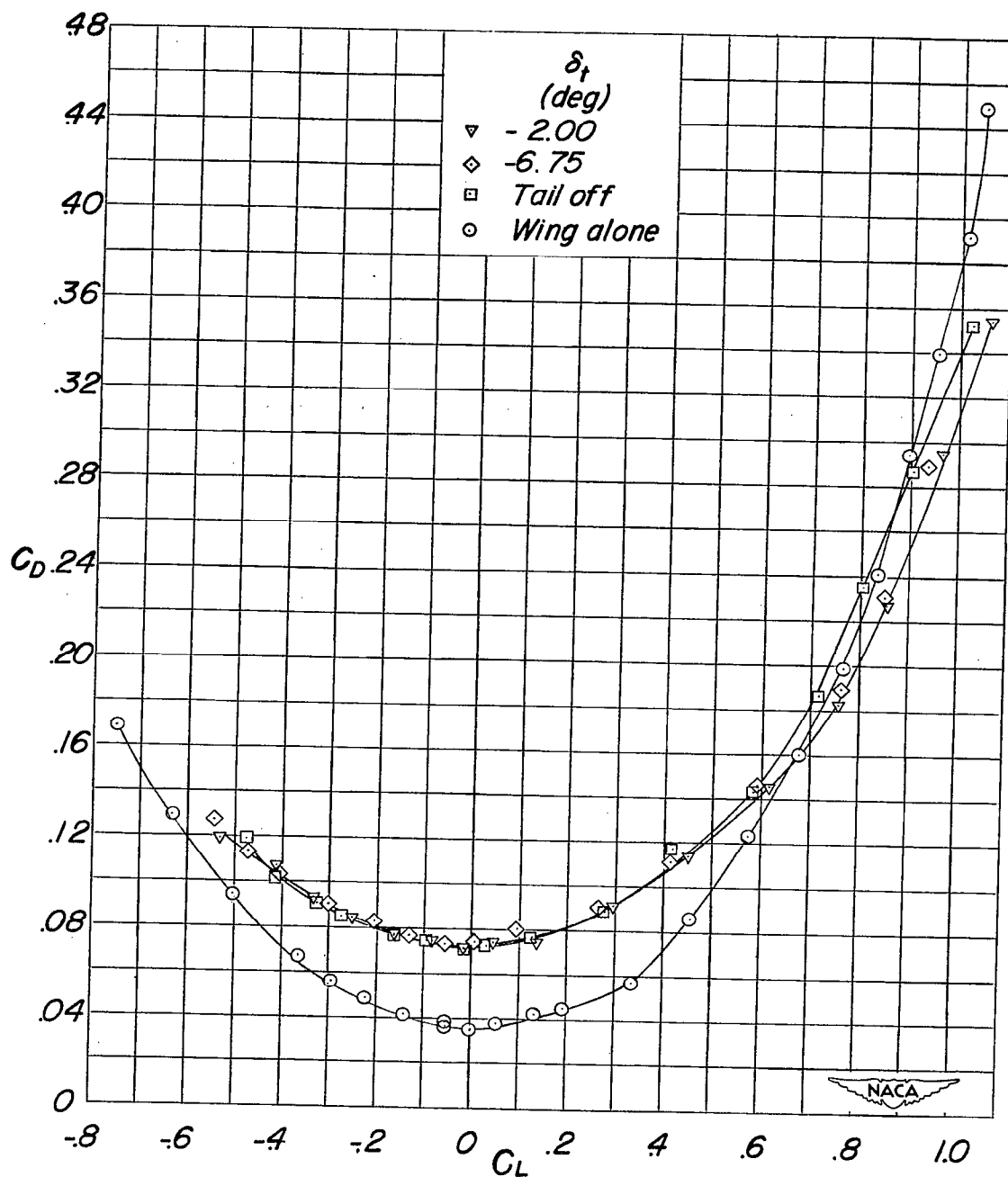
~~CONFIDENTIAL~~(h) $M = 1.05$ - Concluded.

Figure 5.- Continued.

~~CONFIDENTIAL~~

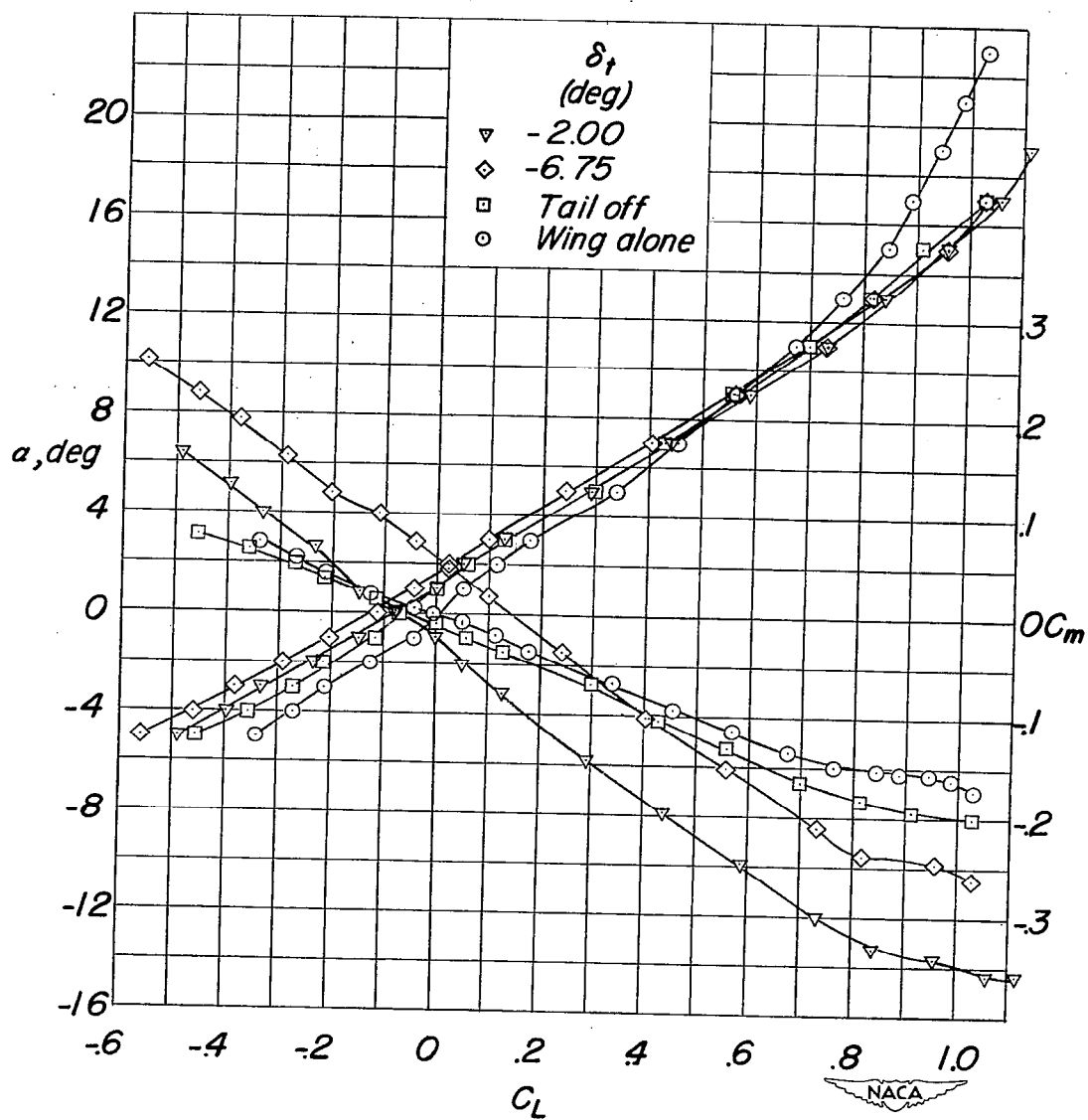
~~CONFIDENTIAL~~(1) $M = 1.10$.

Figure 5.- Continued.

~~CONFIDENTIAL~~

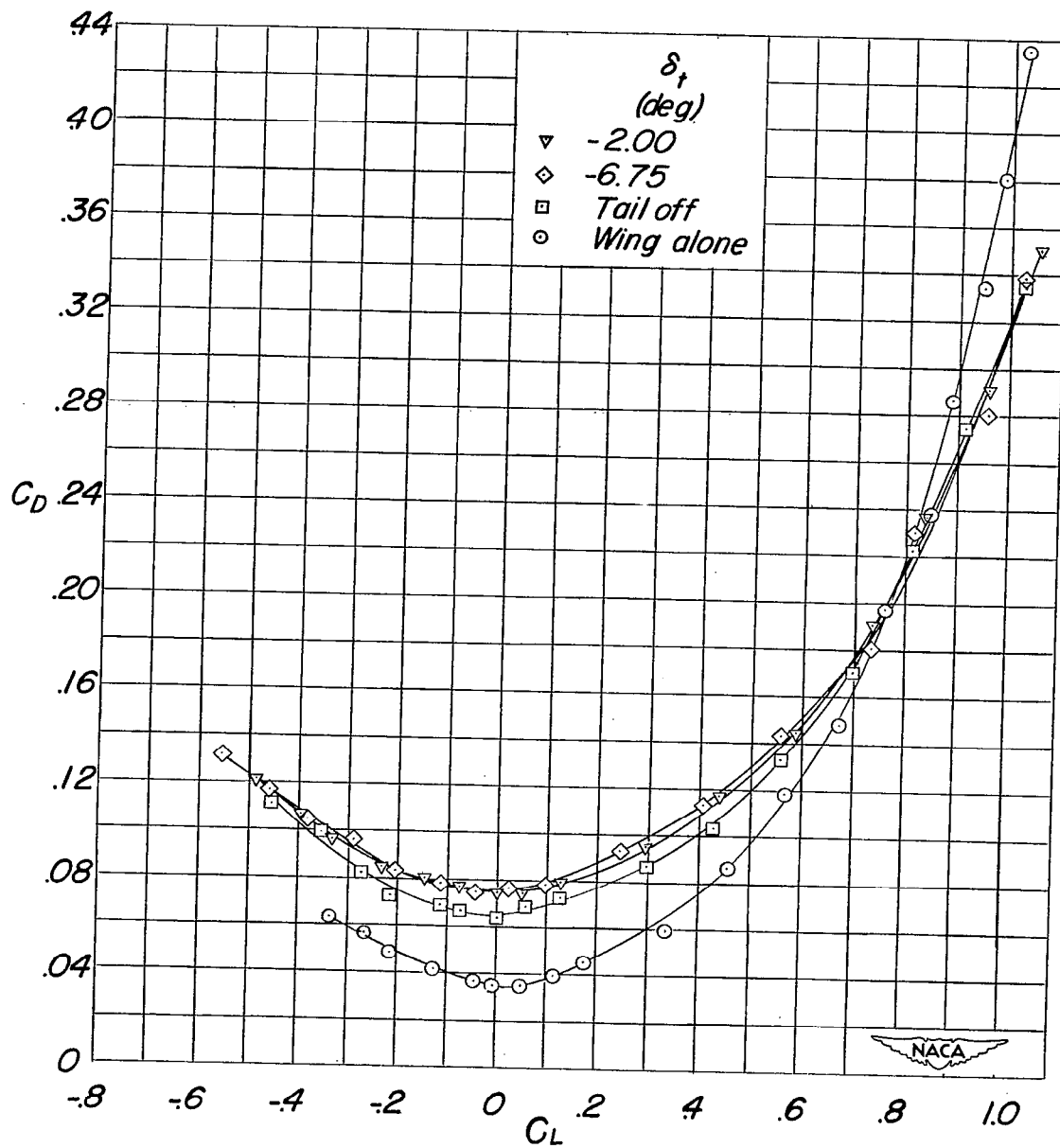
~~CONFIDENTIAL~~(1) $M = 1.10$ - Concluded.

Figure 5.- Continued.

~~CONFIDENTIAL~~

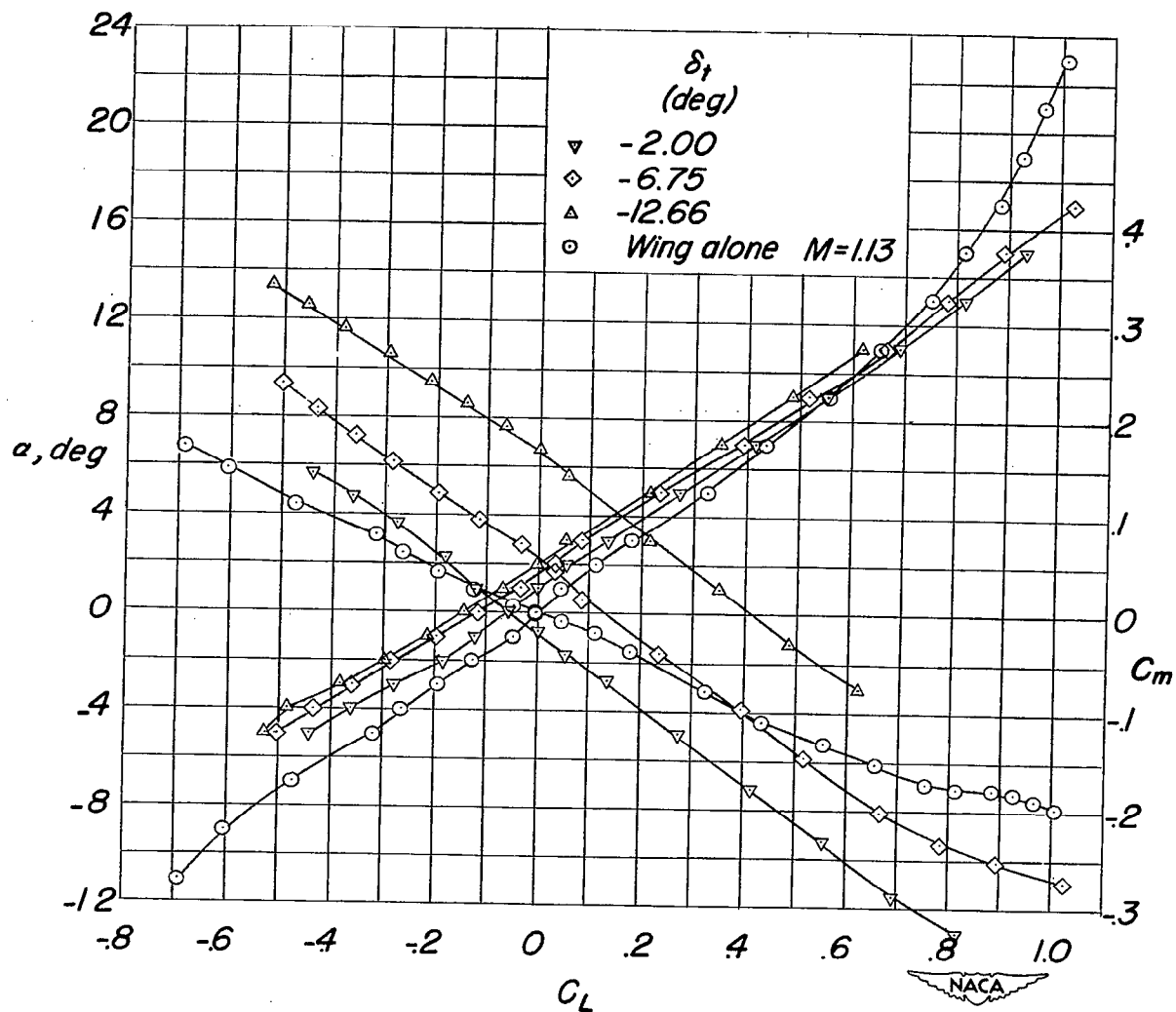
(j) $M = 1.16$.

Figure 5.- Continued.

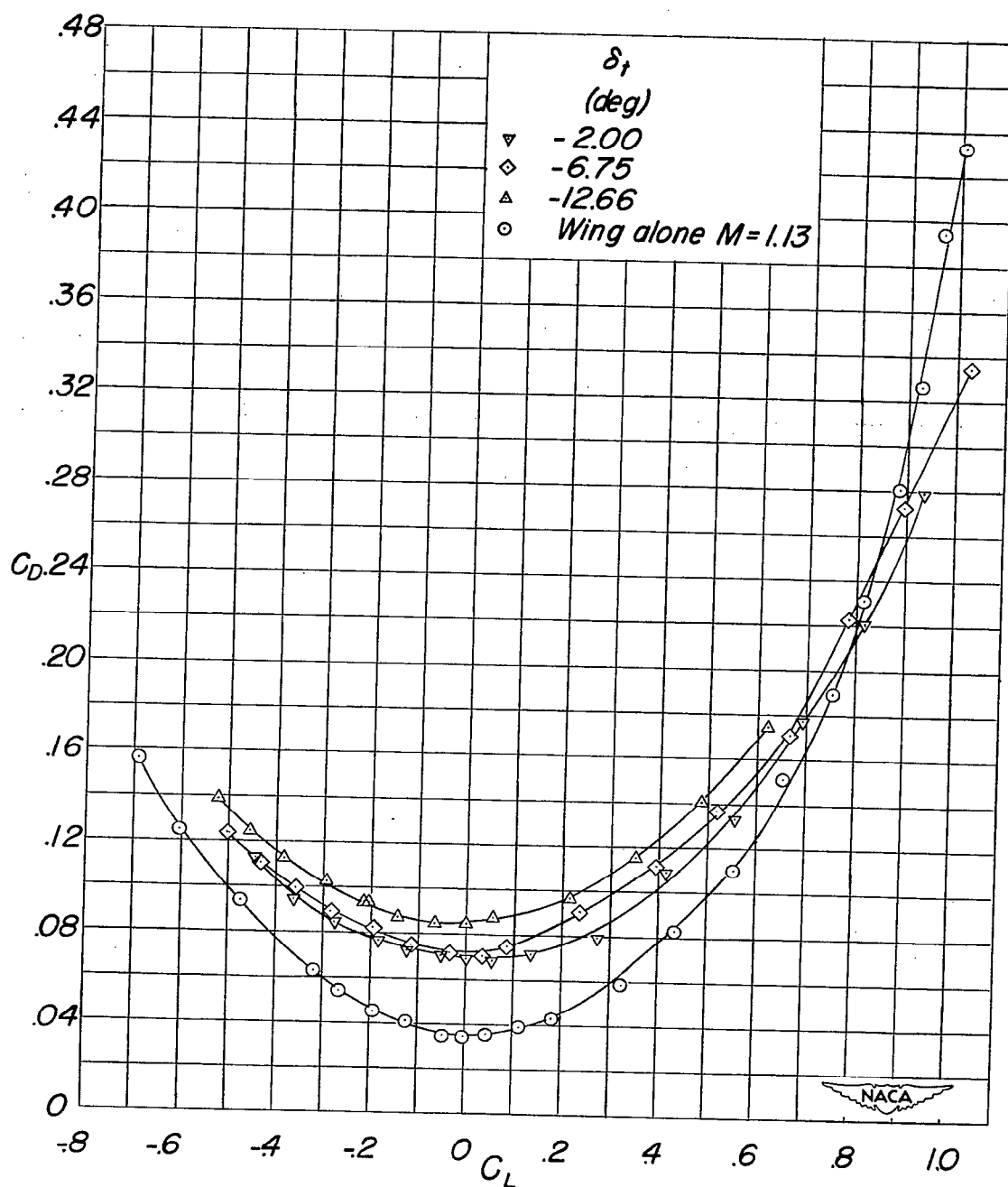
~~CONFIDENTIAL~~(j) $M = 1.16$ - Concluded.

Figure 5.- Concluded.

~~CONFIDENTIAL~~

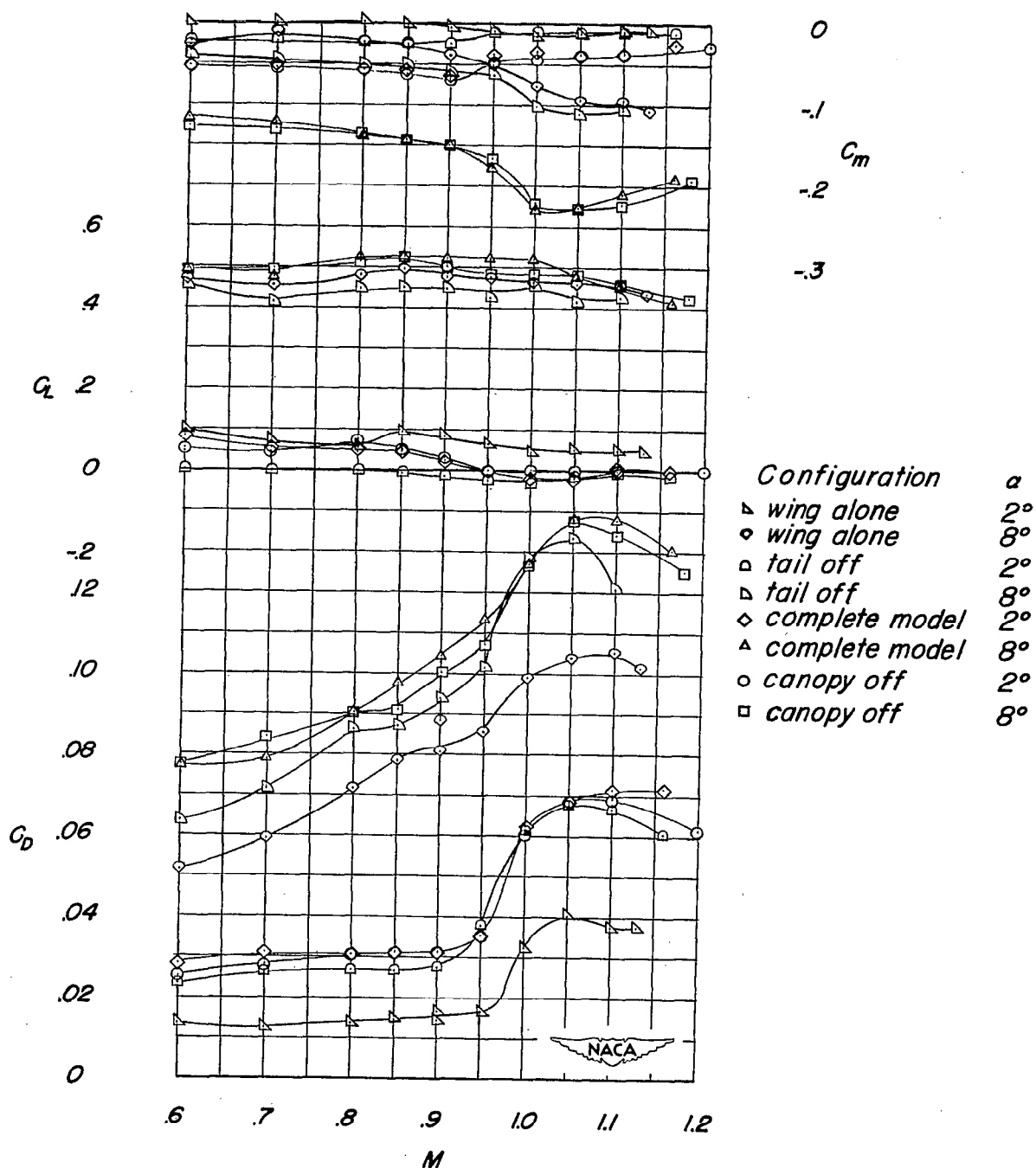


Figure 6.- The effect of the model components on the longitudinal aerodynamic characteristics of the test model.

~~CONFIDENTIAL~~

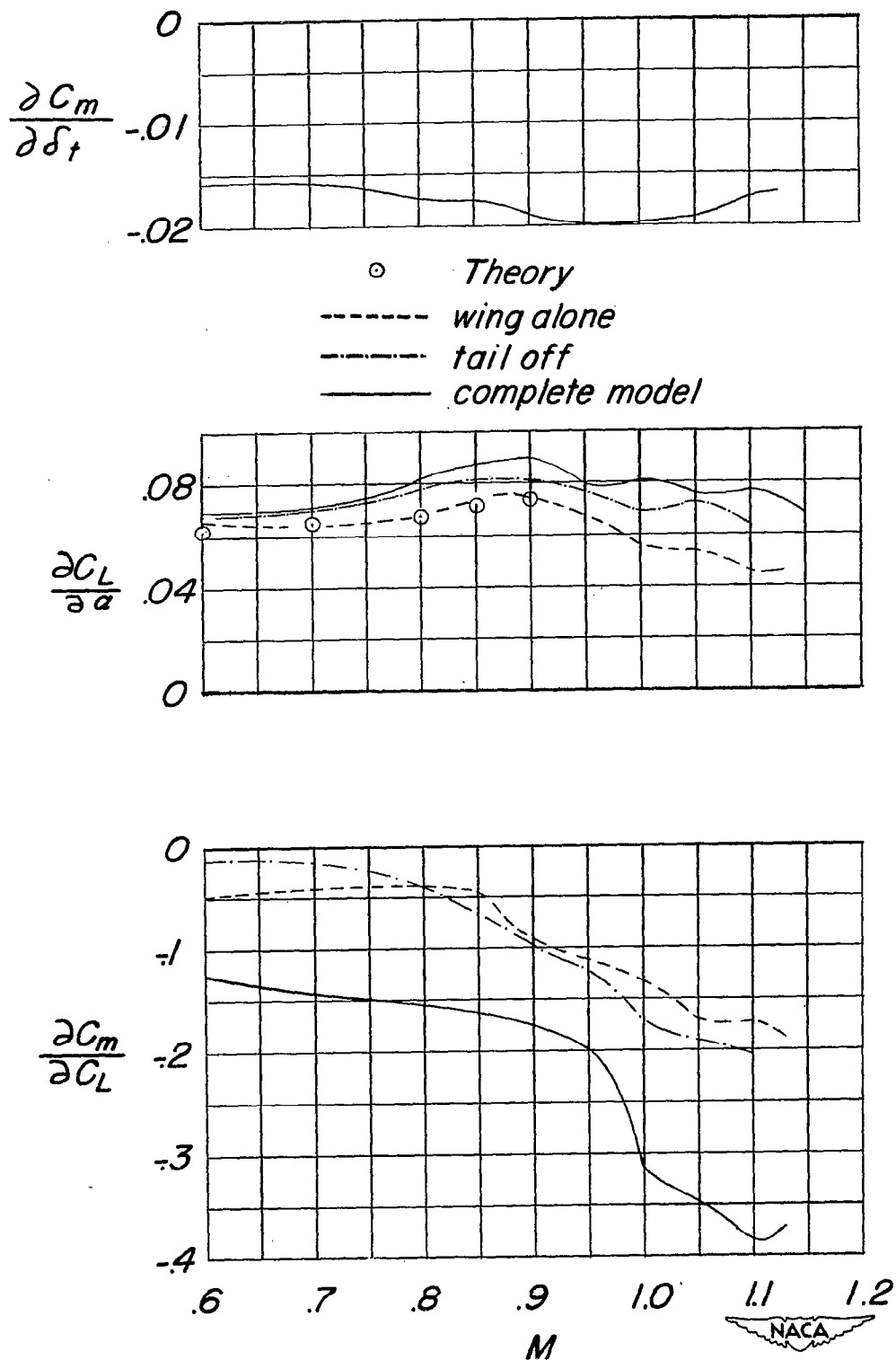


Figure 7.- The longitudinal parameters of the test model.

~~CONFIDENTIAL~~

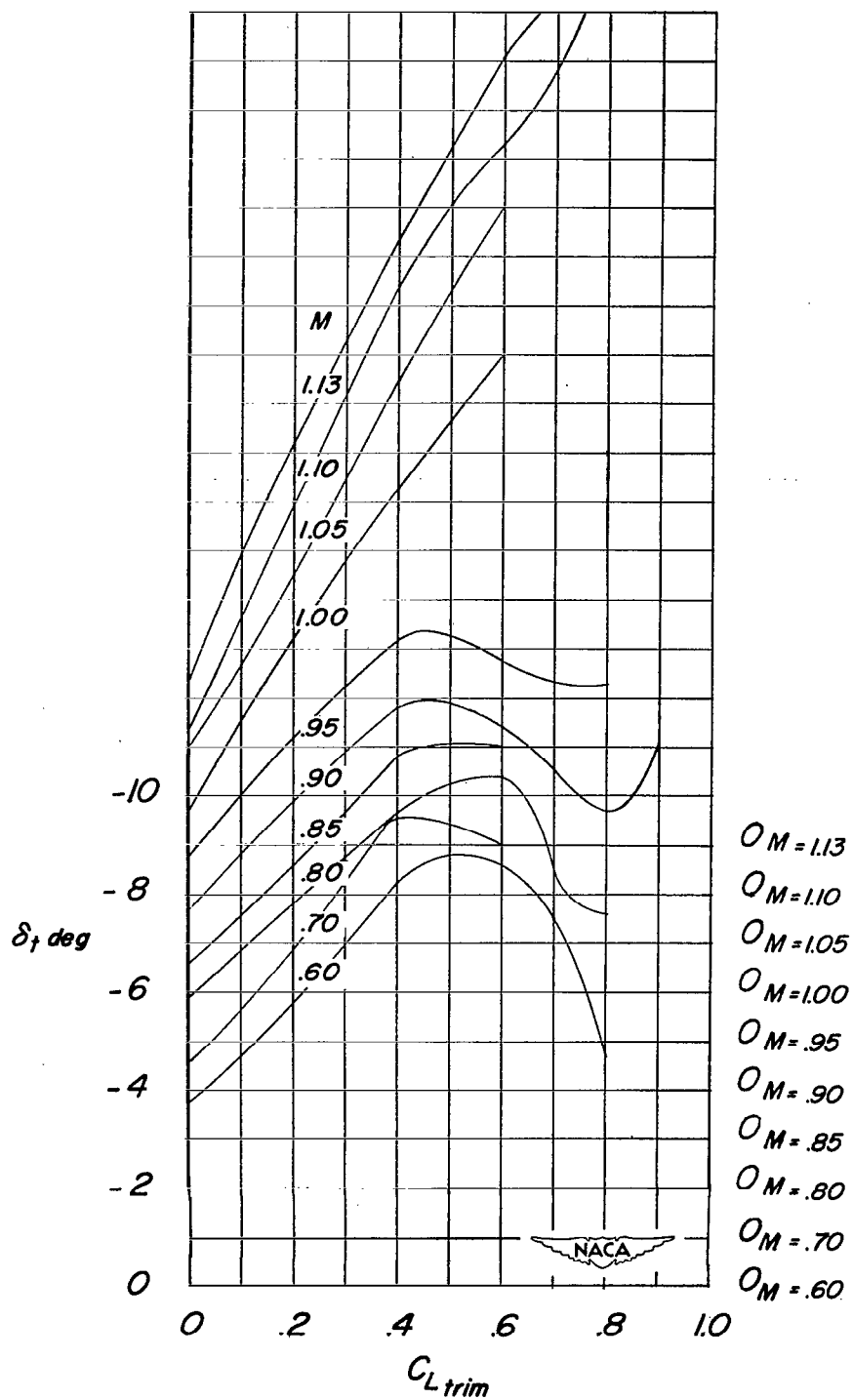
~~CONFIDENTIAL~~

Figure 8.- The tail incidence required for $C_{L_{trim}}$ at various Mach numbers for the model.

~~CONFIDENTIAL~~

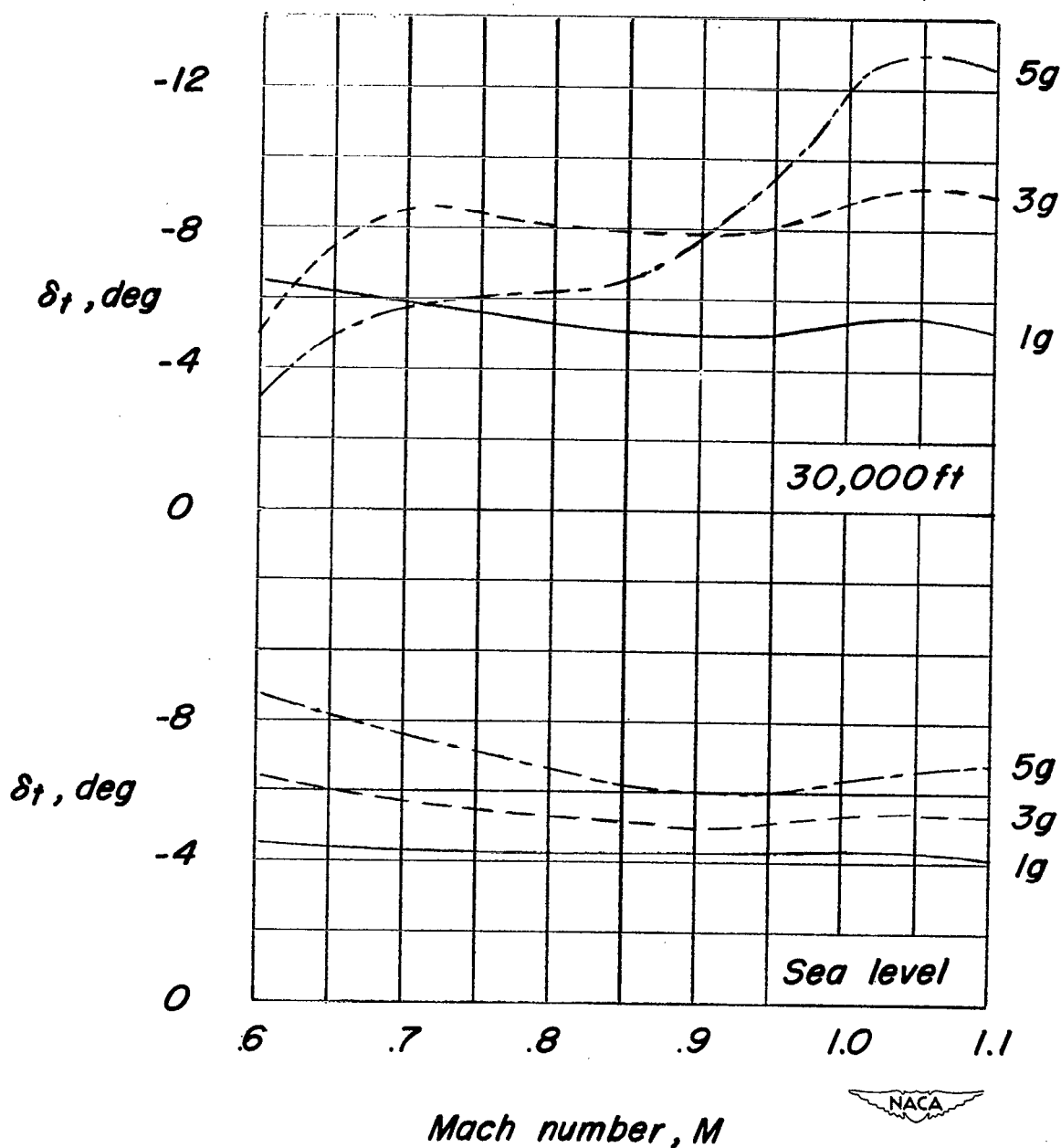
~~CONFIDENTIAL~~

Figure 9.- Tail incidence required for accelerated maneuvers (pull-ups) at various Mach numbers for the Skate 9 seaplane as estimated from tests of a $\frac{1}{80}$ -scale semispan model. Wing loading, 42.5 pounds per square foot.

~~CONFIDENTIAL~~

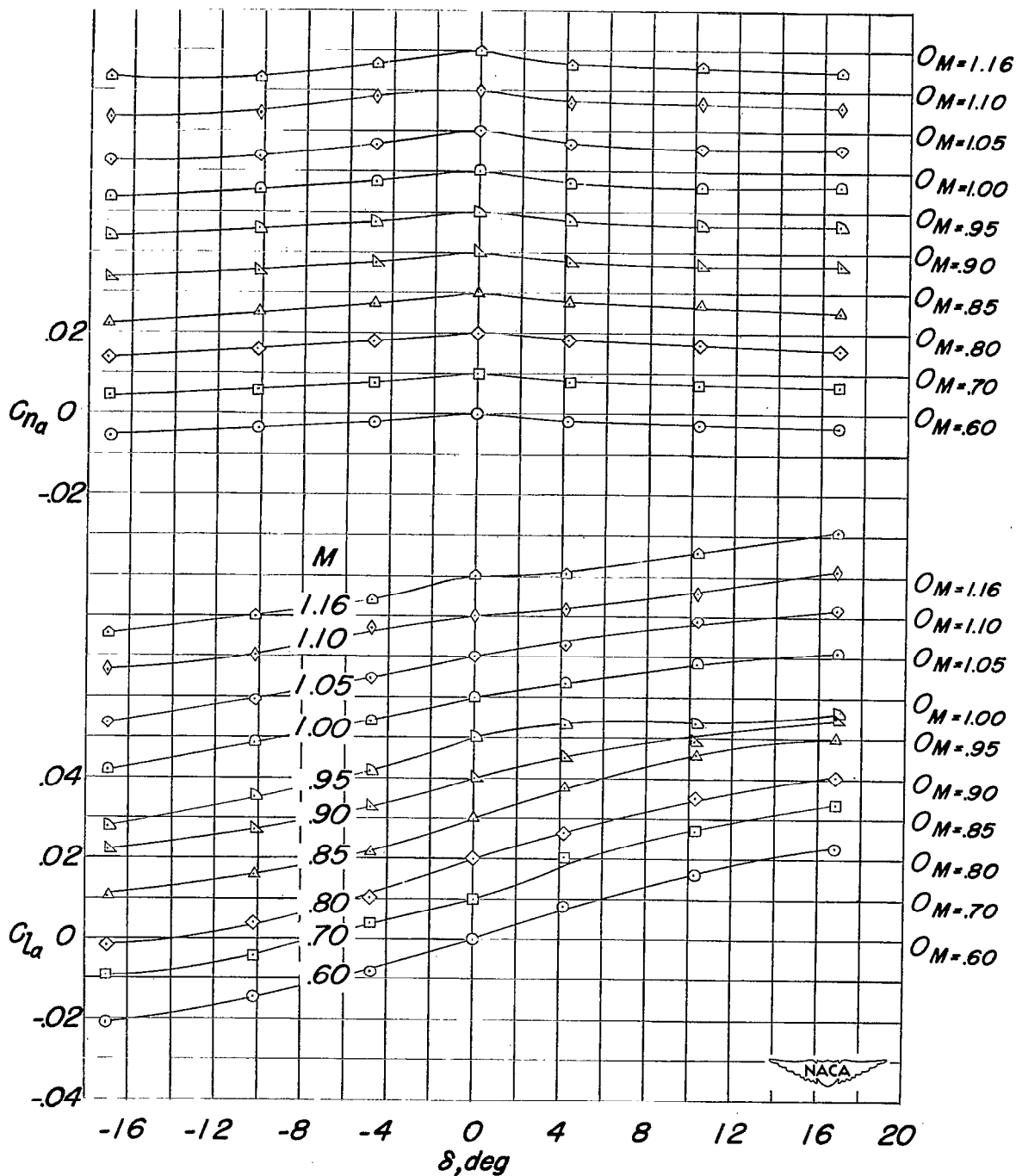
(a) $\alpha = -4^\circ$.

Figure 10.- The aileron characteristics of the test model.

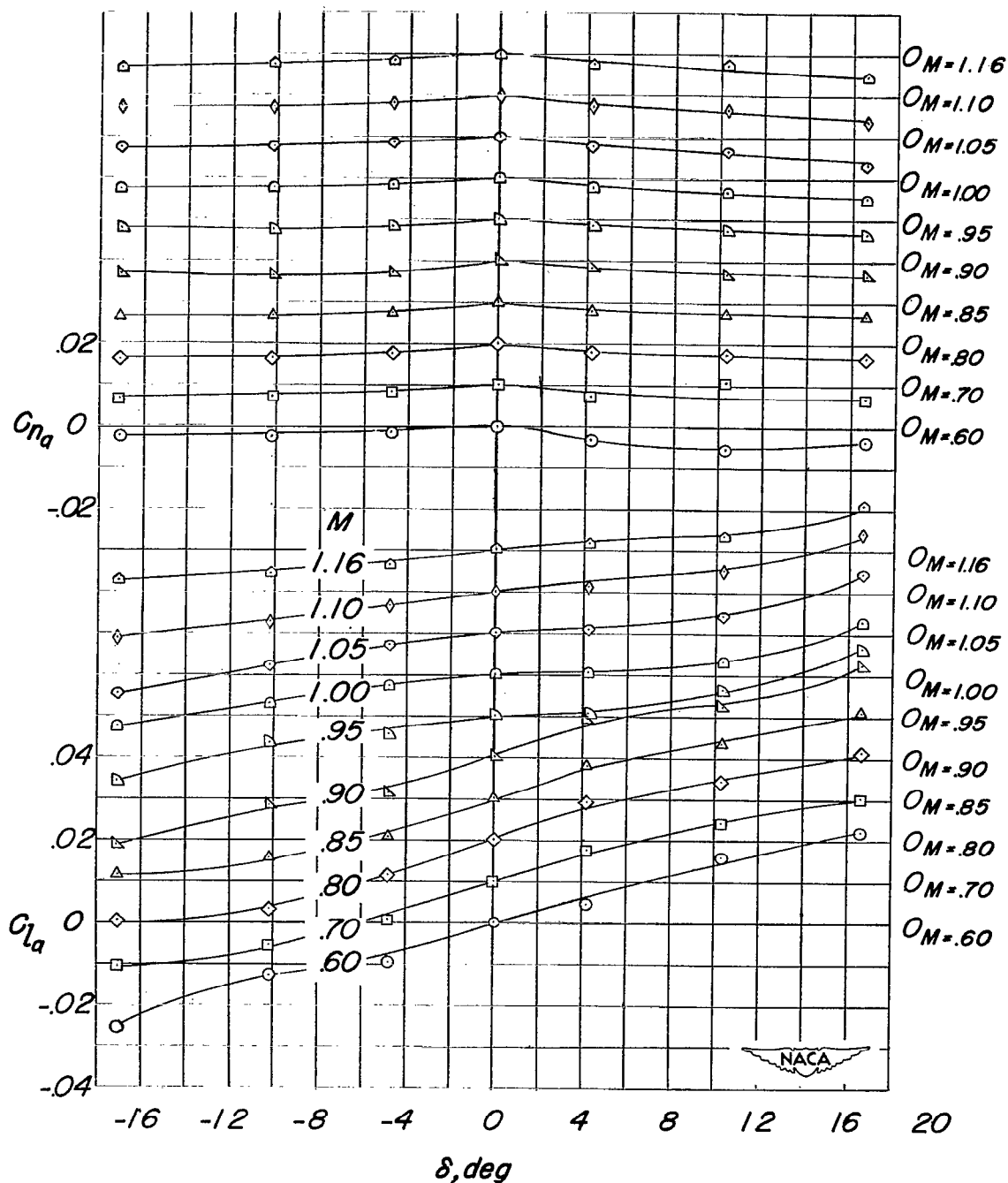
~~CONFIDENTIAL~~(b) $\alpha = 2^\circ$.

Figure 10.- Continued.

~~CONFIDENTIAL~~

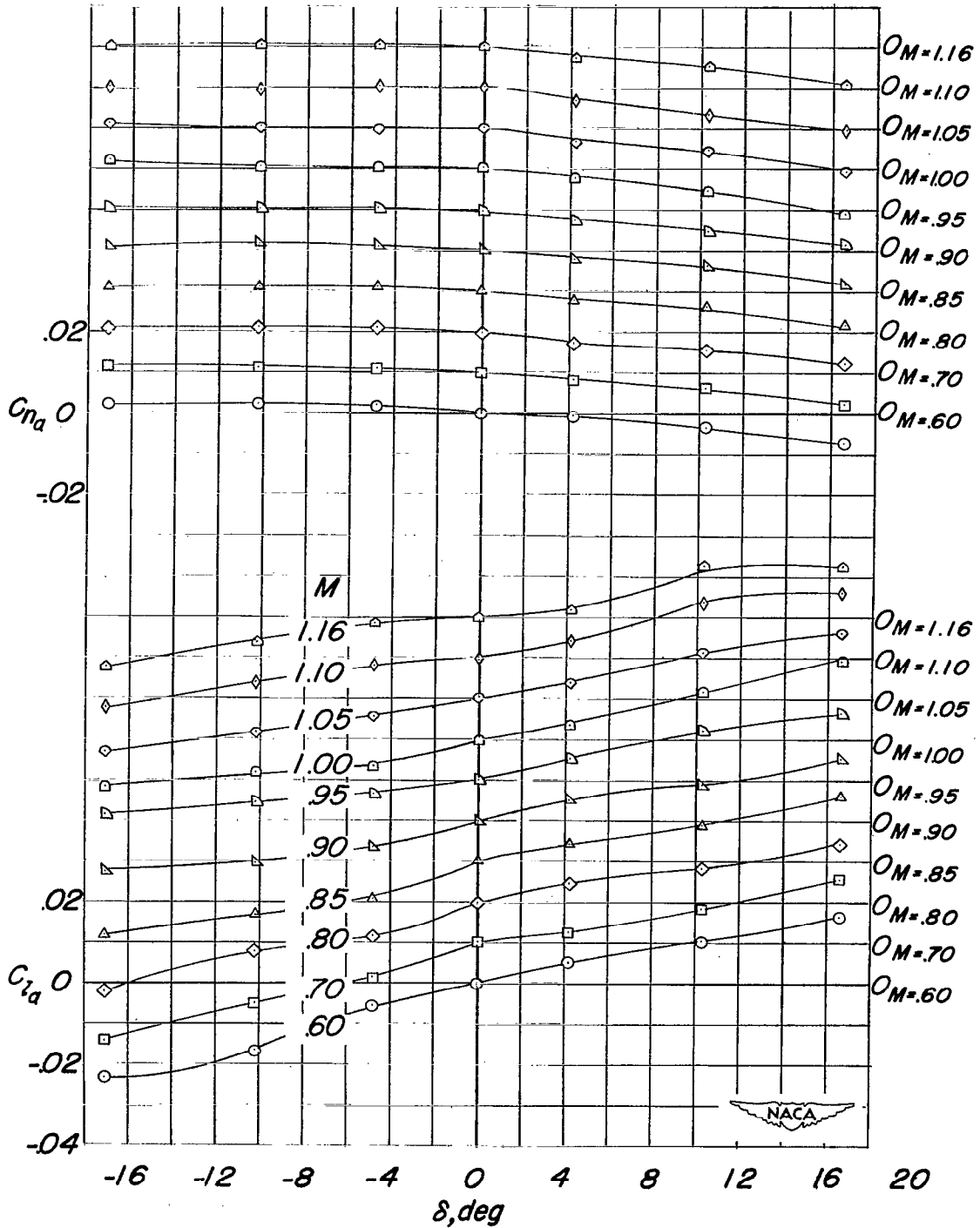
(c) $\alpha = 8^\circ$.

Figure 10.- Continued.

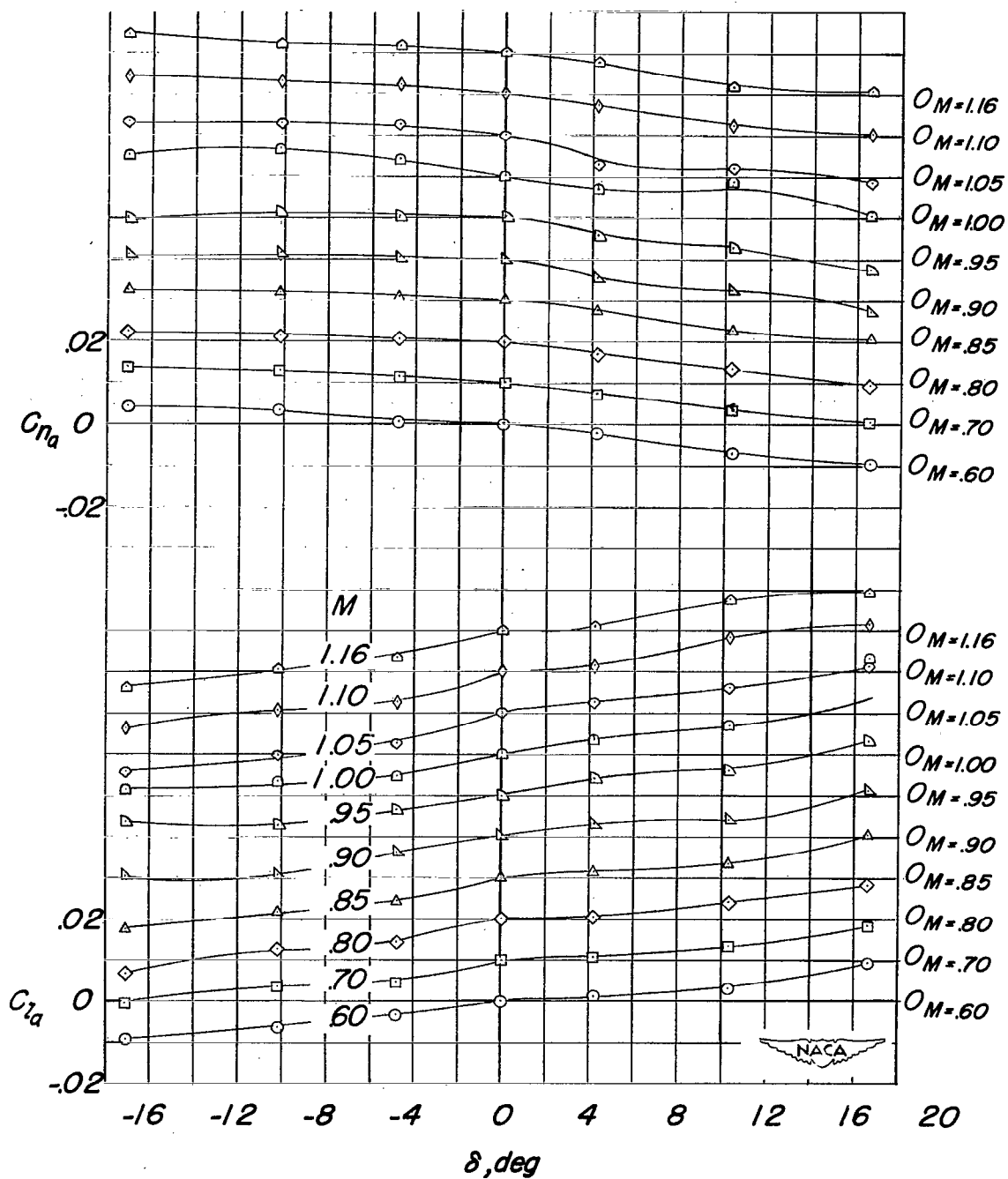
~~CONFIDENTIAL~~(d) $\alpha = 16^\circ$.

Figure 10.- Concluded.

~~CONFIDENTIAL~~

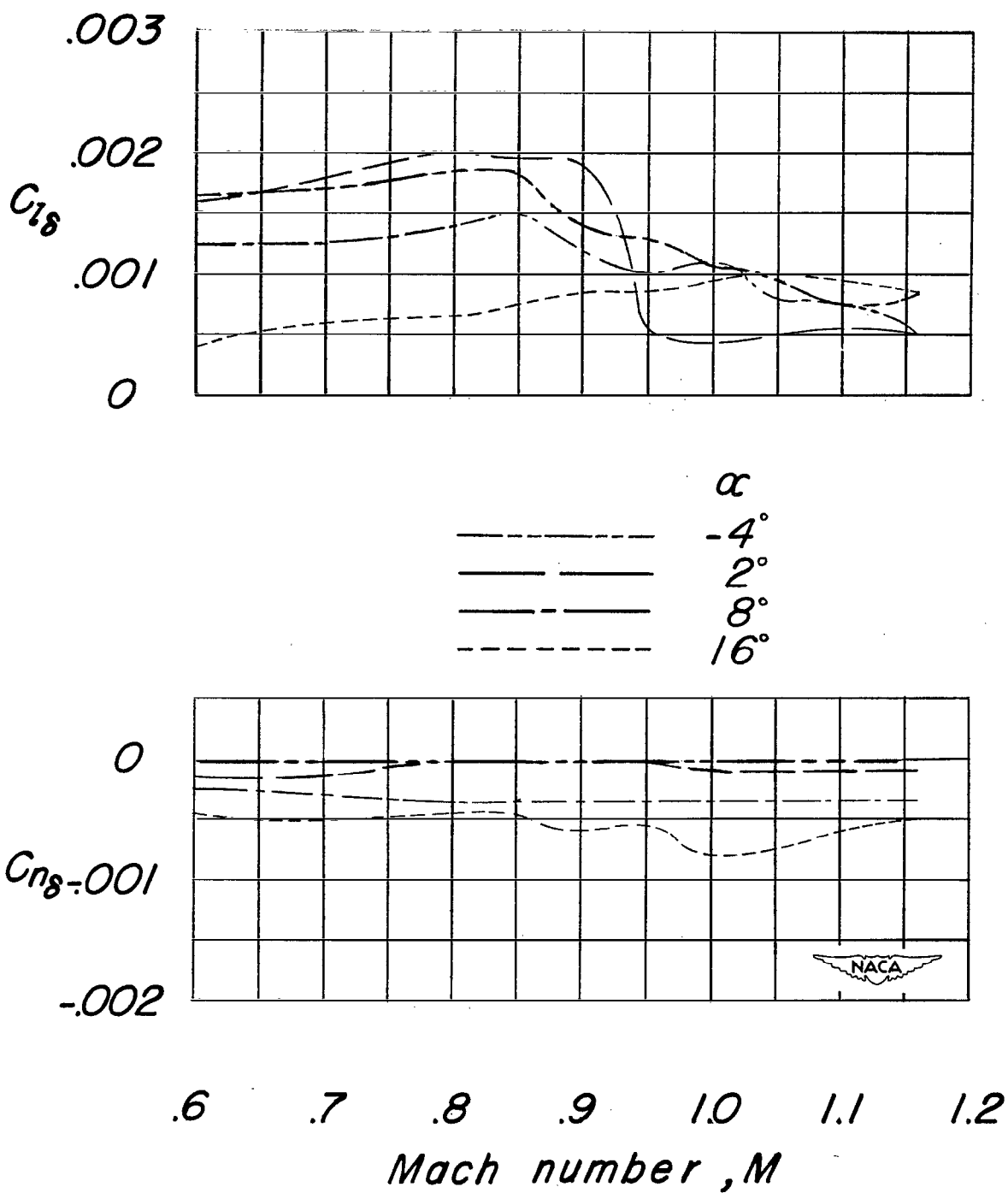
~~CONFIDENTIAL~~

Figure 11.- The aileron parameters of the test model.

~~CONFIDENTIAL~~

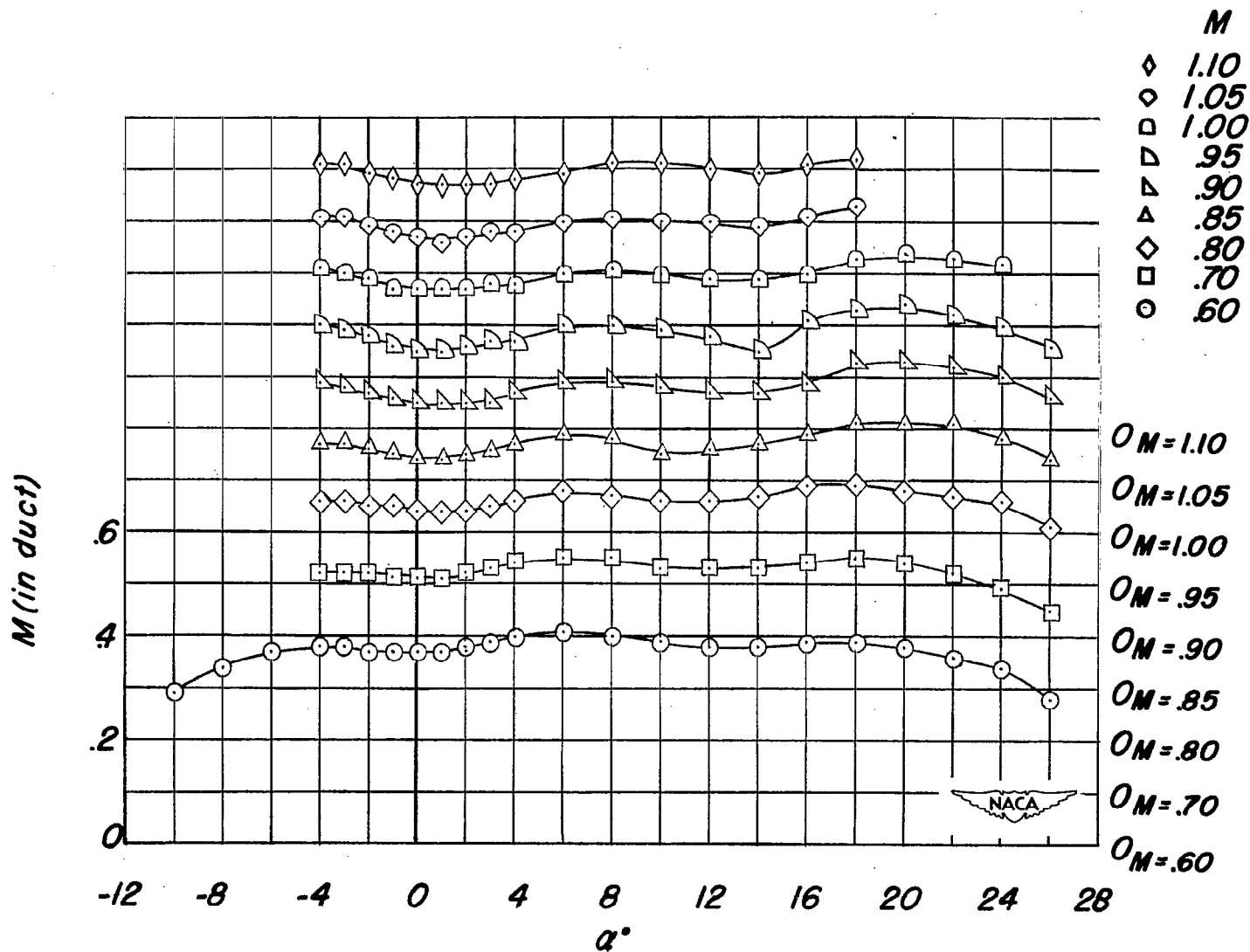


Figure 12.- The variation of the Mach number in the duct with angle of attack of the test model.

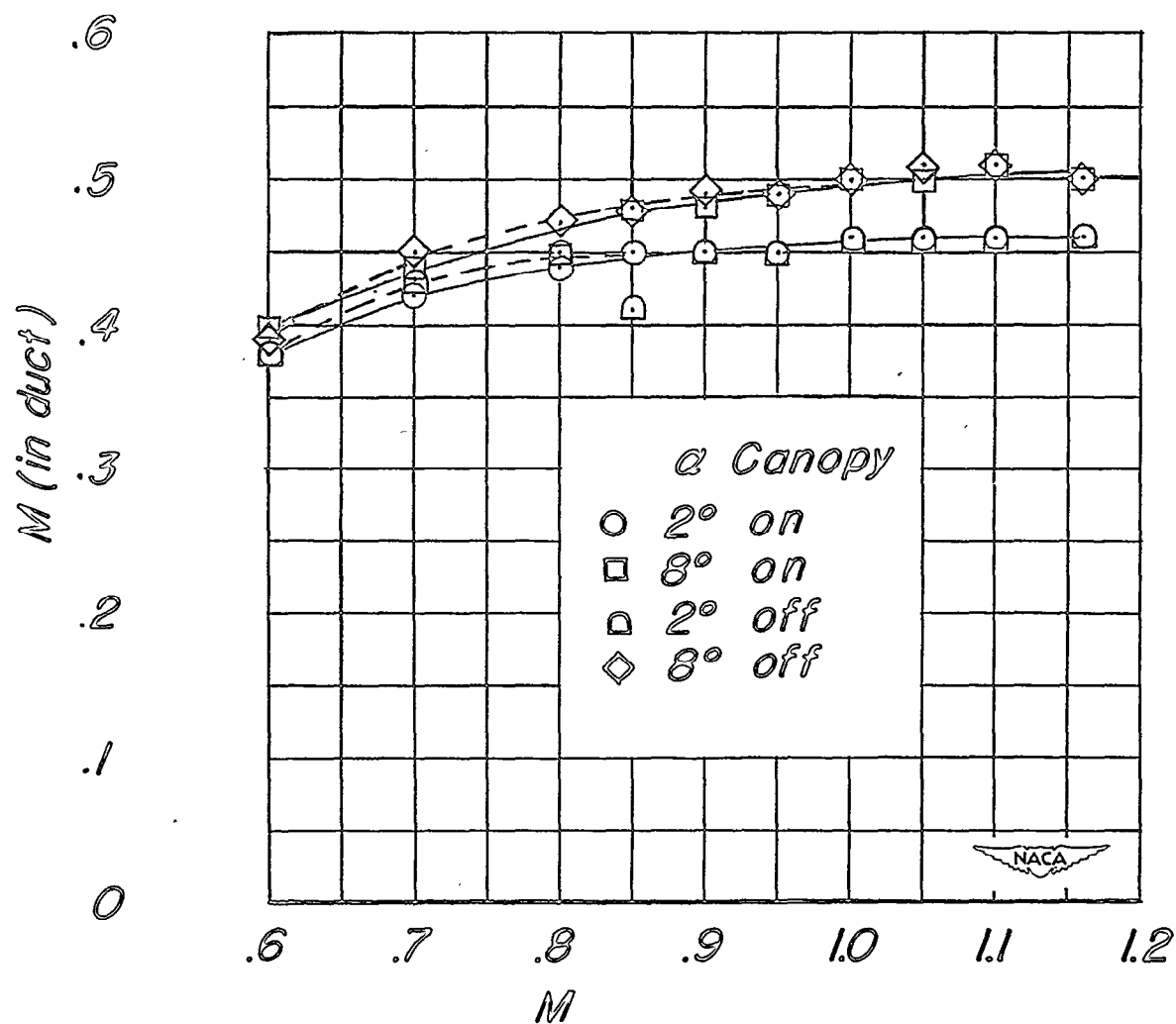


Figure 13.- The effect of the canopy on the variation of the Mach number in the duct with the test Mach number.



$M = 1.00; \alpha = 0^\circ.$



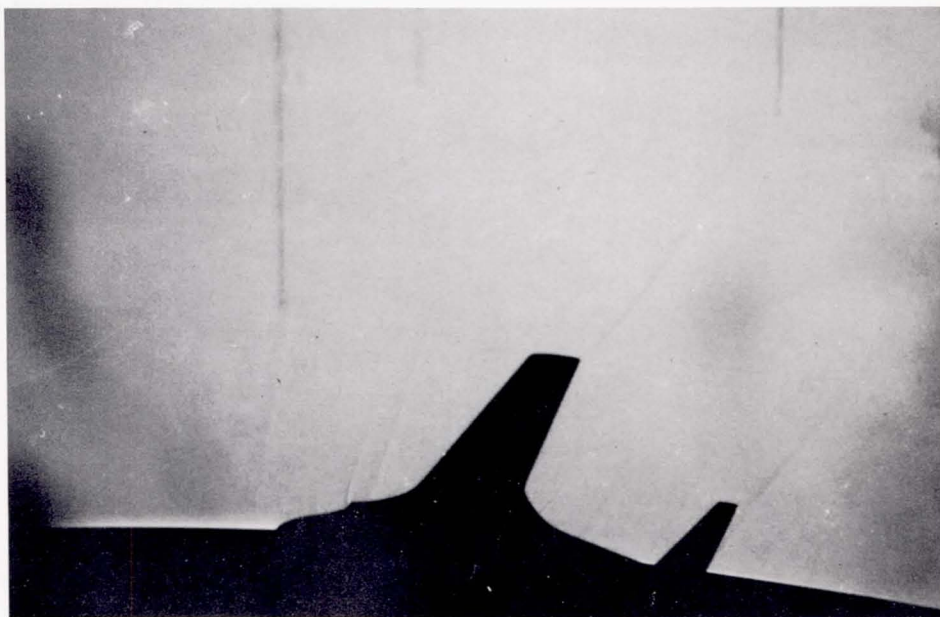
$M = 1.05; \alpha = 0^\circ.$

NACA
L-70757

Figure 14.- Shock patterns over test model in position on transonic bump.



$M = 1.10; \alpha = 0^\circ.$



$M = 1.16; \alpha = 0^\circ.$

Figure 14.- Continued.

NACA
L-70758



$M = 1.16; \alpha = 8^\circ.$

Figure 14.- Concluded.

NACA
L-70759

NASA Technical Library



3 1176 01438 6123